Motif-Based Hypergraph Representation Learning: Transductive and Inductive Inference for Gene Regulatory Networks

Songyang Wu, Mingjing Tang, Tong Zi, Lin Liu, Shaojie Qiao, Guiguang Ding, *Senior Member, IEEE*, and Wei Gao

***Abstract*—Network motifs, as fundamental functional substructures in gene regulatory networks (GRNs), play a critical role in regulating gene expression. Despite the successful application of graph representation learning in GRN modeling, most existing approaches mainly capture pairwise relationships and overlook higher order regulatory patterns encoded by functional motifs, which limits the accuracy of regulatory inference. To address this limitation, we propose Motif-GRN, a motif-based hypergraph representation learning framework that captures the underlying biological logic in higher order semantic structures. We first identify statistically significant regulatory motifs and construct a multichannel motif-induced hypergraph. We then design a motif-aware hypergraph convolutional network to extract motif-centric semantic features, while a conventional graph convolution module preserves first-order relational information. In addition, we introduce cross-view contrastive learning to align heterogeneous representations and enhance gene embeddings. Building on Motif-GRN, we develop an inductive extension that enables cross-dataset generalization and effective GRN inference with limited labels. Extensive experiments on three ground-truth networks across seven cell types demonstrate that Motif-GRN outperforms state-of-the-art baselines in both transductive and inductive GRN inference tasks, highlighting its potential for higher order regulatory network modeling.**

***Index Terms*—Biological network inference, gene regulatory network (GRN), hypergraph representation learning, network motif.**

Received 27 September 2025; revised 11 February 2026; accepted 13 April 2026. This work was supported in part by the Key Project of Basic Research in Yunnan Province under Grant 202501AS070007; in part by the National Natural Science Foundation of China under Grant U2002204, Grant 62472370, and Grant 62262072; in part by the Major Science and Technology Project of Yunnan Province under Grant 202402AD080002; in part by the National Key Research and Development Program of China for Young Scientists under Grant 2022YFF1002500; and in part by the Project Funding of the Support Program of Xingdian Talents. *(Corresponding author: Mingjing Tang.)*

Songyang Wu is with the School of Information Science and Technology, Yunnan Normal University, Kunming 650500, China, and also with the School of Computer and Artificial Intelligence, Southwest Jiaotong University, Chengdu 611756, China (e-mail: wsy@my.swjtu.edu.cn).

Mingjing Tang is with the School of Information Science and Technology, Yunnan Normal University, Kunming 650500, China, and also with the Ministry of Education, Engineering Research Center for High-Value Utilization of Yunnan's Characteristic Biological Resources, Kunming 650500, China (e-mail: tmj@ynnu.edu.cn).

Tong Zi and Lin Liu are with the School of Information Science and Technology, Yunnan Normal University, Kunming 650500, China (e-mail: zeeetong@163.com; liulinrachel@163.com).

Shaojie Qiao is with the School of Software Engineering, Chengdu University of Information Technology, Chengdu 610225, China (e-mail: sjqiao@cuit.edu.cn).

Guiguang Ding is with the School of Software, BNRist, THUIBCS, BLBCI, Tsinghua University, Beijing 100084, China (e-mail: dinggg@tsinghua.edu.cn).

Wei Gao is with the School of Mathematics, Hohai University, Nanjing 211100, China (e-mail: gaowei@hhu.edu.cn).

Digital Object Identifier 10.1109/TNNLS.2026.3685617

I. Introduction

GENE expression regulation is a fundamental mechanism underlying phenotypic variation in biological systems [1]. To elucidate how transcription factors (TFs) cooperate with target genes to orchestrate transcriptional processes, systems biologists often refer to these interactions as gene regulatory networks (GRNs) [2], [3]. Systematic analysis of GRNs helps clarify molecular mechanisms in biology and underpins advances in disease research, including tumorigenesis [4], therapeutic target discovery [5], [6], and personalized precision medicine [7], [8].

To characterize the complex dependencies between TFs and target genes, various computational models have been proposed. Traditional unsupervised statistical and machine learning methods [9], [10], [11], [12] predominantly rely on expression data to infer gene-level associations but often neglect prior regulatory knowledge. Recently, supervised deep learning frameworks [13], [14], [15], [16] have emerged, which integrate epigenetic modifications and other biological priors, leading to substantial advances in modeling gene regulatory relationships. However, despite their success, most existing approaches fundamentally model GRNs as collections of independent pairwise TF–gene interactions, making it difficult to explicitly capture cooperative and higher order regulatory dependencies among multiple genes.

This limitation is particularly problematic because gene transcription often involves the coordinated response of multiple genes. Such relationships recur in GRNs as subgraphs with specific topological features, known as network motifs. Shen-Orr et al. [17] first introduced this concept, showing that the *E. coli* GRN is assembled from multiple motifs in a "Lego-like" manner. Motivated by this, we used the mfinder program [18] to systematically detect and evaluate three-node motifs in human and mouse ground-truth networks. Fig. 1 presents the motif significance distribution in the Nonspecific ChIP-seq dataset, where motifs with Z-score $>$ 2 are considered statistically significant [19]. Across both

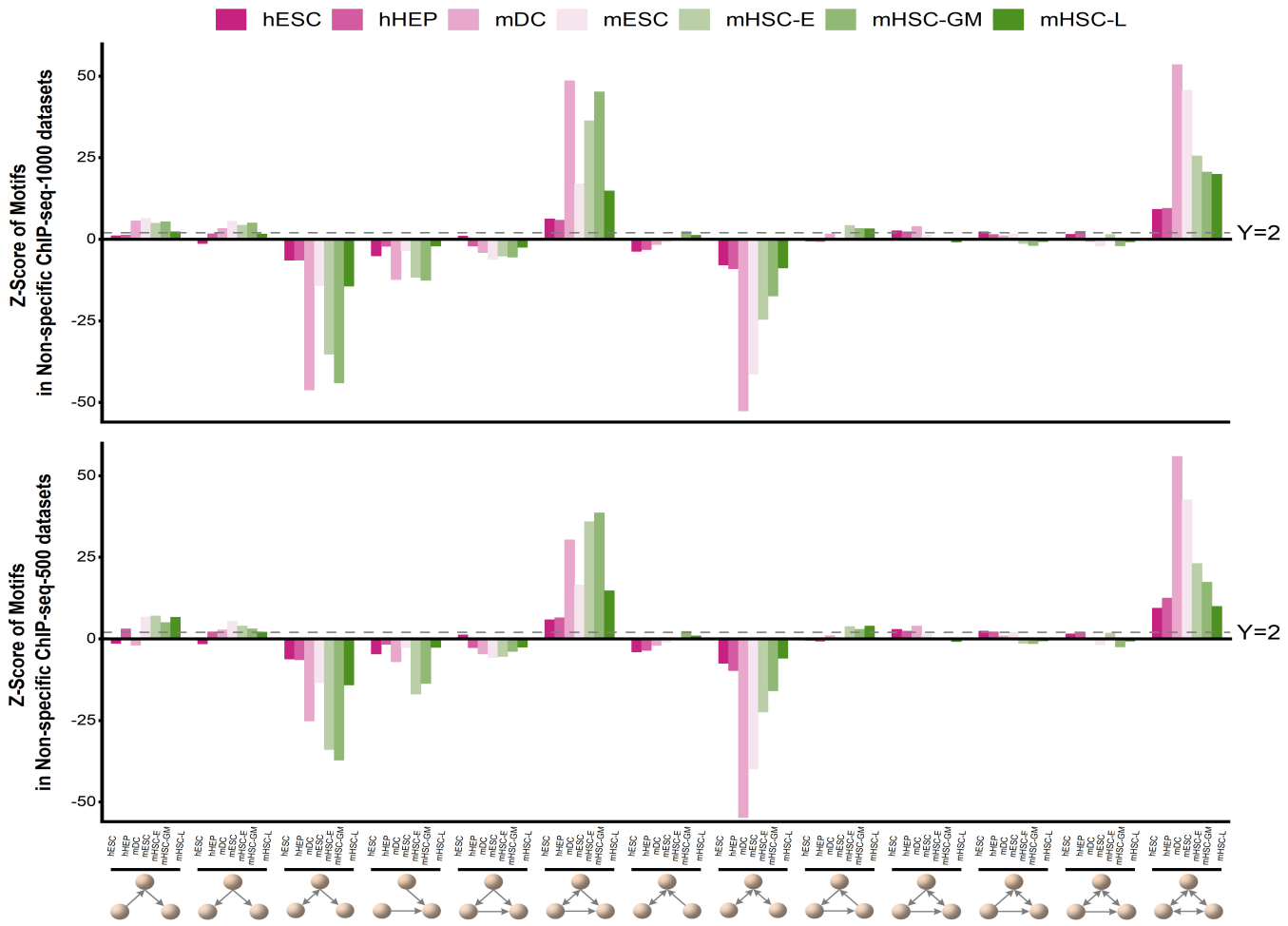

Fig. 1. Statistical significance analysis of three-node motifs across ground-truth networks in the Nonspecific ChIP-seq dataset. Motifs are identified using mfinder, and their significance is evaluated based on Z-score criteria. The x-axis represents seven scRNA-seq datasets and thirteen motif types, while the y-axis shows motif Z-scores. A gray dashed line indicates the significance threshold at Z-score = 2.

ChIP-seq-500 and ChIP-seq-1000 networks, a substantial proportion of three-node motifs consistently exhibit statistically significant enrichment, while additional motifs show moderate enrichment above random expectation. Detailed statistics are reported in Supplementary Tables S1–S21, with visual summaries in Figs. S1 and S2. These observations indicate that network motifs are not incidental local patterns but constitute fundamental and reusable higher order regulatory building blocks in GRNs. Nevertheless, most current GRN inference methods remain largely pairwise-focused [11], [12], [15], [16] and lack a principled mechanism to incorporate motif-level higher order semantics into representation learning frameworks.

To explicitly bridge this gap between statistically significant regulatory motifs and computational GRN inference, we propose Motif-GRN, a motif-aware hypergraph representation learning framework that systematically integrates motif-level higher order regulatory semantics into GRN inference. We first perform statistical enrichment analysis on all three-node motifs in GRNs and select the most significant types as templates to construct a motif-induced multichannel hypergraph, where each channel corresponds to a biologically meaningful regulatory pattern. Then, Motif-GRN employs a motif-aware hypergraph convolutional network to capture higher order semantic structures within motifs and a conventional GCN to model direct pairwise interactions. To mitigate the information homogenization caused by the direct fusion of features from different structural views, we design a cross-view self-supervised contrastive learning mechanism. Finally, we obtain unified embeddings of genes to predict regulatory associations. Moreover, we develop an inductive extension of Motif-GRN, enabling cross-dataset generalization and addressing the scarcity of regulatory annotations in certain organisms.

The main contributions of this work are summarized as follows.

1) We present the first multichannel motif-aware hypergraph neural network to model recurrent subgraph structures in GRNs. By introducing a novel construction strategy for motif-induced hypergraph adjacency, the proposed framework effectively captures the biological semantics of higher order regulation.
2) The proposed Motif-GRN model integrates a motif-driven hypergraph encoder with a conventional graph encoder to jointly capture higher order cooperative semantics and direct regulatory relationships and

introduces a cross-view self-supervised task to improve the consistency of gene representations across views.

3) We further design the first inductive hypergraph framework for GRN inference, supporting cross-dataset training and testing generalization and effectively alleviating the challenge posed by limited prior regulatory knowledge.
4) Extensive evaluations conducted on multiple datasets demonstrate that Motif-GRN consistently outperforms state-of-the-art methods in terms of AUROC and AUPRC, thereby validating its effectiveness and broad applicability in both transductive and inductive GRN inference tasks.

II. Related Work

A. GRN Inference Methods

Inspired by the "guilt-by-association" principle [20], correlation-based methods assume co-expression between upstream TFs and downstream genes, using correlation coefficients to capture linear [11] or nonlinear [12] regulatory relationships. Information-theoretic approaches employ entropy [21], mutual information, and conditional mutual information [22], [23] to reveal statistical dependencies in gene expression. Regression-based models [24], [25] express target gene levels as functions of multiple TFs, where coefficients indicate regulatory strength and direction. However, these unsupervised approaches heavily rely on expression data and often fail to incorporate prior regulatory signals such as epigenetic modifications. Convolutional neural network (CNN) [26] methods like CNNC [13] transform the prior regulatory pairs into histograms to uncover latent patterns, and CNNGRN [14] further integrates network topology with expression data to enhance spatial feature extraction. Despite this, CNNs struggle to capture contextual semantics and are computationally intensive. Given the intrinsic graph structure of GRNs, graph neural networks (GNNs) [27] have emerged as powerful tools, improving reconstruction accuracy and interpretability. For example, GRGNN [15] formulates regulatory inference as subgraph classification; GENELink [16] applies graph attention networks (GATs) to infer dependencies from incomplete data; and GNNLink [28] models GRN reconstruction as link prediction using graph convolutional networks. In [29], multisubgraph CNNs are proposed to integrate complementary biological networks. Recent studies have further enhanced GNN-based GRN inference by introducing residual structures and attention mechanisms, such as GRANet, which improves the modeling of complex regulatory dependencies through graph residual attention [30]. Overall, graph deep learning captures local and global regulatory structures via neighborhood aggregation but mainly models explicit pairwise relationships between TFs and target genes, making it difficult to represent synergistic effects among multiple genes directly [31], [32], [33].

B. Higher Order Modeling in Biological Networks

Complex biological networks, including gene regulatory, protein–protein interaction, and metabolic networks, often exhibit higher order interactions that go beyond simple pairwise relations. Hypergraphs provide a natural framework for capturing such multinode dependencies [34], [35], [36]. Recently, hypergraph neural networks have been widely developed for general higher order representation learning and applied to multimodal data integration and node classification tasks. For example, DHHNN leverages dynamic hypergraph structures and variational learning to model higher order interactions across multiple domains [37]. However, most hypergraph-based representation learning methods still focus primarily on structural connectivity while remaining limited in their ability to encode biological semantics.

In contrast, network motifs—subgraph patterns with specific functions—offer an alternative means of analyzing the higher order structures of biological networks. Typical three- or four-node motifs, such as feed-forward loops (FFLs) and bi-fans, are prevalent in biological systems, including gene regulatory and signaling pathways [17]. Existing studies [38] indicate that, from bacteria to humans, various motifs perform specific signal processing functions in GRN. However, most current studies focus solely on the statistical properties of motifs and rarely integrate them systematically into representation learning frameworks. This gap limits the characterization of their structural roles and semantic contributions. Recent advances have attempted to integrate motif information into GNNs. For instance, Zhang et al. [39] introduced MGSSL, a self-supervised framework leveraging molecular motifs for pretraining, while Liu et al. [40] developed the MARS model, which employs a motif-based generation strategy for reaction center identification and synthon completion in chemical reaction prediction. These studies highlight the potential of motif-driven modeling in complex biochemical systems. Nevertheless, most existing methods rely on edge-level decomposition or implicit encoding of subgraph patterns, which undermines the preservation of cooperative multinode semantics and restricts their capacity to capture higher order regulatory logic. In contrast, Motif-GRN explicitly treats statistically significant regulatory motifs as biologically interpretable higher order structural units and incorporates them into motif-induced hypergraph representations, enabling the modeling of cooperative gene regulation with improved interpretability.

III. Methods

A. Motif-GRN Framework

Motif-GRN is a novel framework for GRN reconstruction that leverages motif-induced hypergraphs to capture structural and functional modules underlying transcriptional regulation. As illustrated in Fig. 2, the architecture consists of three key components.

1) *Multichannel Motif-Induced Hypergraph Construction:* Ten representative motifs are selected based on statistical significance analysis across ground-truth networks to construct distinct hypergraph channels, each representing a biologically meaningful higher order regulatory pattern;

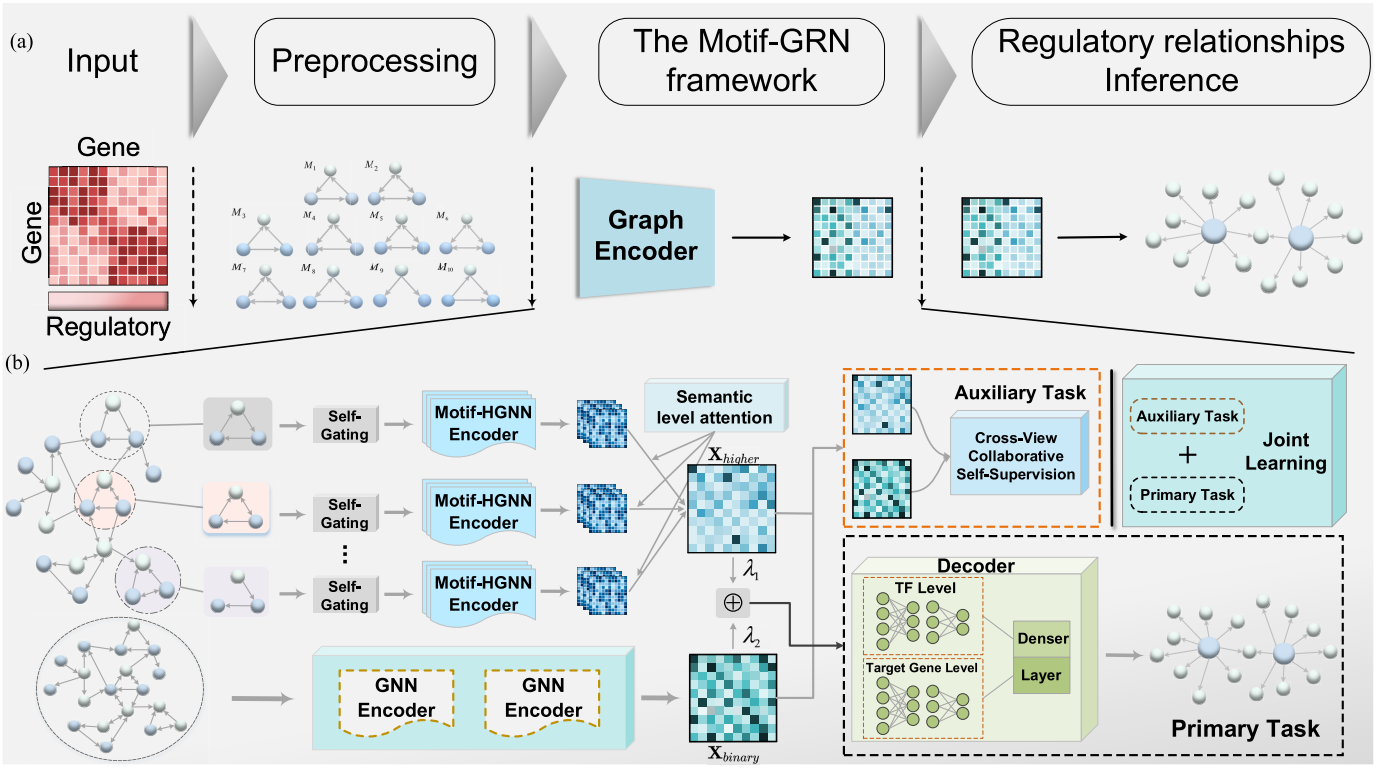

Fig. 2. Overview of the Motif-GRN workflow. (a) Illustration of the overall pipeline, from learning gene representations based on prior regulatory data to inferring potential gene regulatory relationships. (b) Proposed framework consists of three main stages: 1) constructing motif-induced multichannel hypergraphs to capture higher order regulatory semantics; 2) learning high-order semantic features ($\mathbf{X}_{higher}$) and explicit pairwise regulatory features ($\mathbf{X}_{binary}$) via parallel hypergraph and graph encoders, respectively, with cross-view contrastive self-supervised alignment; and 3) directly integrating the two complementary representations and inferring gene regulatory dependencies through an inner product decoder to reconstruct the GRN.

2) *Joint Representation Learning of Higher Order and Pairwise Interactions:* A motif-aware hypergraph encoder is designed to extract semantic features from higher order regulatory structures, while a GNN encoder is employed in parallel to capture explicit pairwise regulatory interactions between genes.
3) *Cross-View Self-Supervised Contrastive Learning:* Semantic and structural features from both encoders are aligned using a self-supervised contrastive learning strategy. Auxiliary objectives are jointly optimized with the downstream task to enhance multiview gene representations and improve GRN reconstruction performance.

B. Construction of Motif-Induced Hypergraphs

To capture higher order interactions among genes, we construct a hypergraph based on the prior regulatory network, where hyperedges are defined by statistically enriched recurring subgraph patterns, rather than entity types. Specifically, we identify a set of highly enriched three-node motifs within the regulatory network that reflect distinct many-to-many regulatory relationships and use them to construct a multichannel motif-induced hypergraph. As illustrated in Fig. 3(a), we select ten representative motifs by integrating their enrichment properties with their canonical functional roles in transcriptional regulatory networks [36], with each motif encoding a distinct and functionally interpretable regulatory pattern. For example, in the FFL motif, regulator A controls gene C both directly and indirectly via gene B. This structure enhances the system's robustness by filtering out transient signals, ensuring that gene C is activated only in response to sustained regulation from A.

1) Network Motif Definition: A motif M is defined as a tuple $(\mathbf{K}, \mathcal{A})$ with n nodes, where $\mathbf{K}$ is an $n \times n$ binary adjacency matrix, and $\mathcal{A} \subset \{1, 2, \ldots, n\}$ denotes the set of participating nodes. In this study, we focus on directed three-node motifs, which serve as fundamental regulatory building blocks. Fig. 3(b) presents an example motif, illustrating both its structural pattern and formal representation.

2) Motif-Induced Adjacency Matrix: Given a specific motif type M_k, the co-occurrence frequency of genes i and j within its instances $\mathcal{M}_k$ effectively characterizes higher order regulatory relationships. The motif-induced adjacency matrix $\mathbf{A}_{M_k}$ is defined as

$$\mathbf{A}_{M_k}(i, j) = \sum_{i \neq j} \mathbb{I}(i, j \text{ occur in the same instance of } \mathcal{M}_k) \tag{1}$$

where $\mathbb{I}(\cdot)$ is the indicator function returning 1 if genes i and j co-occur in a motif instance, and 0 otherwise. Here, $\mathbf{A}_{M_k}(i, j)$ denotes the frequency with which nodes i and j co-occur within the same instance of motif M_k across the entire network. As illustrated in Fig. 3(c), a five-node graph is used to demonstrate the motif-induced adjacency matrix for motif M_3, where $\{1, 2, 3\}$ and $\{1, 2, 5\}$ represent two instances of motif M_3.

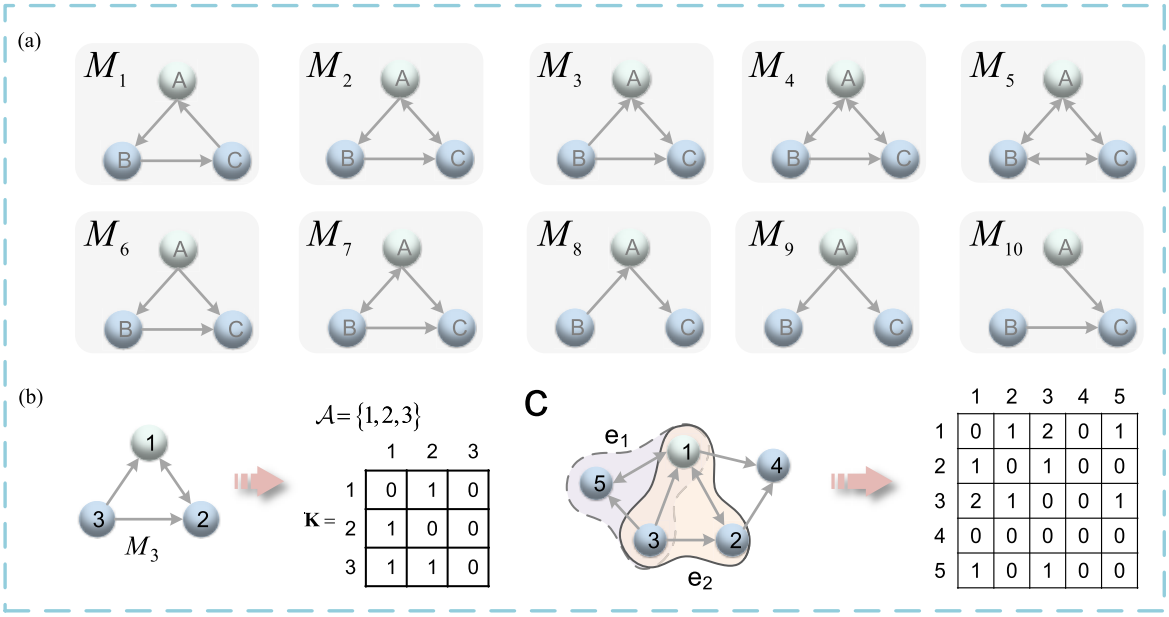

Fig. 3. (a) Ten selected three-node network motifs used in this study. (b) Instance of motif M_3, along with its corresponding node set $\mathcal{A}$ and binary adjacency matrix $\mathbf{K}$. (c) Five-node directed graph (left) and the motif-induced adjacency matrix for M_3 (right).

TABLE I
COMPUTATION RULES OF MOTIF-INDUCED HYPERGRAPH ADJACENCY MATRIX $\mathbf{A}_{M_t}$

Motif	Matrix Operation	$\mathbf{A}_{M_t}$
M_1	$\mathbf{C}=(\mathbf{UU})\odot\mathbf{U}^\top$	$\mathbf{C}+\mathbf{C}^\top$
M_2	$\mathbf{C}=(\mathbf{BU})\odot\mathbf{U}^\top+(\mathbf{UB})\odot\mathbf{U}^\top+(\mathbf{UU})\odot\mathbf{B}$	$\mathbf{C}+\mathbf{C}^\top$
M_3	$\mathbf{C}=(\mathbf{BB})\odot\mathbf{U}+(\mathbf{UB})\odot\mathbf{B}+(\mathbf{UB})\odot\mathbf{B}$	$\mathbf{C}+\mathbf{C}^\top$
M_4	$\mathbf{C}=(\mathbf{BB})\odot\mathbf{B}$	$\mathbf{C}$
M_5	$\mathbf{C}=(\mathbf{UU})\odot\mathbf{U}+(\mathbf{UU}^\top)\odot\mathbf{U}+(\mathbf{U}^\top\mathbf{U})\odot\mathbf{U}$	$\mathbf{C}+\mathbf{C}^\top$
M_6	$\mathbf{C}=(\mathbf{UB})\odot\mathbf{U}+(\mathbf{BU}^\top)\odot\mathbf{U}^\top+(\mathbf{U}^\top\mathbf{U})\odot\mathbf{B}$	$\mathbf{C}$
M_7	$\mathbf{C}=(\mathbf{U}^\top\mathbf{B})\odot\mathbf{U}^\top+(\mathbf{BU})\odot\mathbf{U}+(\mathbf{U}^\top\mathbf{U})\odot\mathbf{B}$	$\mathbf{C}$
M_8	$\mathbf{C}=\mathbf{UU}^\top$	$\mathbf{C}+\mathbf{C}^\top$
M_9	$\mathbf{C}=\mathbf{SS}^\top$	$\mathbf{C}$
M_{10}	$\mathbf{C}=\mathbf{S}^\top\mathbf{S}$	$\mathbf{C}$

3) Motif-Induced Hypergraph: Hypergraphs generalize traditional graphs by allowing hyperedges to connect multiple nodes, making them well-suited for modeling higher order regulatory structures. We define a motif-induced hypergraph as $\mathcal{G}=(V,E)$, where V is the set of gene nodes and E is the set of hyperedges, each corresponding to an instance of a three-node regulatory motif. To represent higher order gene interactions, we use a hypergraph incidence matrix $\mathbf{H}\in\mathbb{R}^{|V|\times|E|}$, where $\mathbf{H}(v,e)=1$ if gene v is part of hyperedge e, and 0 otherwise.

As shown in Fig. 3(c), the motif instance $\{1,3,5\}$ of motif M_3 corresponds to hyperedge e_1, while $\{1,2,3\}$ forms another hyperedge e_2. In GRNs, the sheer number of motif instances results in an extremely large incidence matrix $\mathbf{H}\in\mathbb{R}^{|V|\times|E|}$, which poses significant computational and storage challenges. To mitigate such computational burden, we adopt the approach from [53] by constructing motif-induced hypergraph adjacency matrices without explicitly storing hyperedges. Given the original adjacency matrix $\mathbf{S}$, we define the bidirectional part as $\mathbf{B}=\mathbf{S}\odot\mathbf{S}^\top$ and the unidirectional part as $\mathbf{U}=\mathbf{S}-\mathbf{B}$, where $\odot$ denotes the Hadamard product. Using these definitions, the motif-induced hypergraph adjacency matrices $\mathbf{A}_{M_t}$ for the ten selected three-node motifs are constructed through a series of matrix operations detailed in Table I.

C. Multichannel Graph Encoding Layer

The study aims to model and analyze ten types of higher order regulatory motifs. To achieve this, we employ a multi-channel motif-aware hypergraph encoder to extract semantic regulatory features embedded in each motif. Since different motifs contribute unequally to gene representation learning, directly using raw features from all channels is suboptimal. Therefore, a self-gated unit (SGU) is introduced to adaptively filter base gene embeddings per channel. This mechanism enables dynamic adjustment of feature representations. The mechanism is defined as follows:

$$\mathbf{X}_t^{(0)}=f_{gate}^t\left(\mathbf{X}^{(0)}\right)=\mathbf{X}^{(0)}\odot\sigma\left(\mathbf{X}^{(0)}\mathbf{W}_g^t+\mathbf{b}_g^t\right). \tag{2}$$

Let $t\in 1,2,\ldots,10$ denote the index of the motif-induced hypergraph channels. Each channel is associated with learnable parameters $\mathbf{W}g^t\in\mathbb{R}^{d\times d}$ and $\mathbf{b}g^t\in\mathbb{R}^d$, where d is the dimension of the input gene embedding $\mathbf{X}^{(0)}$ and $\sigma(\cdot)$ is a nonlinear activation function. The resulting channel-specific embedding is denoted as $\mathbf{X}_t^{(0)}$. To effectively extract higher order semantic regulatory features while maintaining computational efficiency, we adopt the simplified hypergraph convolution framework from [54]. The layer-wise propagation rule is formulated as

$$\mathbf{X}_t^{(l+1)}=\mathbf{D}_t^{-1}\mathbf{H}_t\mathbf{L}_t^{-1}\mathbf{H}_t^\top\mathbf{X}_t^{(l)} \tag{3}$$

where $\mathbf{X}_t^{(l+1)}$ denotes the embedding updated after the $(l+1)$th hypergraph convolution at channel t; $\mathbf{H}_t$ is the incidence matrix of the motif-induced hypergraph; and $\mathbf{D}_t$ and $\mathbf{L}_t$ are the degree diagonal matrices for nodes and hyperedges, respectively.

However, as previously discussed, the number of motif-induced hyperedges in each channel grows exponentially, leading to prohibitive computational and storage costs for constructing the incidence matrix and performing hypergraph convolutions. This renders direct application of conventional hypergraph convolution frameworks infeasible.

During propagation, the term $\mathbf{H}_t^\top \mathbf{X}_t^{(l)}$ aggregates node features into hyperedges, while the multiplication by $\mathbf{H}_t$ maps hyperedge representations back to nodes. Notably, the matrix $\mathbf{H}_t\mathbf{H}_t^\top \in \mathbb{R}^{m\times m}$ encodes the co-occurrence frequency of node pairs within motif instances, where each entry quantifies how often the corresponding pair appears together in the same motif. Ignoring self-loops, $\mathbf{H}_t\mathbf{H}_t^\top$ is equivalent to the motif-induced adjacency matrix $\mathbf{A}_{M_t}$. Thus, the motif-aware hypergraph convolution simplifies to

$$\mathbf{X}_t^{(l+1)} = \widehat{\mathbf{D}}_t^{-1}\mathbf{A}_{M_t}\mathbf{X}_t^{(l)}. \tag{4}$$

Here, $\widehat{\mathbf{D}}_t$ is the degree matrix associated with the motif-induced adjacency matrix $\mathbf{A}_{M_t}$. This formulation effectively circumvents the high cost of explicitly constructing motif-induced incidence matrices, while significantly reducing the computational overhead of hypergraph-based operations. Different types of motif-induced hypergraph channels capture diverse higher order semantic regulatory relationships among genes. However, since the importance of each motif varies in upstream and downstream regulation, we introduce a semantic-level attention mechanism to adaptively aggregate information from multiple motif channels. This allows the generation of more expressive higher order gene representations. The attention computation is defined as follows, where $\mathbf{a} \in \mathbb{R}^d$ and $\mathbf{W}_{\text{att}} \in \mathbb{R}^{d\times d}$ are trainable parameters and $\mathbf{X}_{higher}^{(l+1)}$ denotes the final higher order gene embeddings:

$$\begin{aligned}\alpha_t &= f_{\text{att}}\left(\mathbf{X}_t^{(l+1)}\right) = \frac{\exp\left(\mathbf{a}^\top \mathbf{W}_{att}\mathbf{X}_t^{(l+1)}\right)}{\sum_{t=1}^{10}\exp\left(\mathbf{a}^\top \mathbf{W}_{att}\mathbf{X}_t^{(l+1)}\right)}\\ \mathbf{X}_{higher}^{(l+1)} &= \sum_{t=1}^{10}\left(\alpha_t \mathbf{X}_t^{(l+1)}\right).\end{aligned} \tag{5}$$

Meanwhile, many genes participate predominantly in simple pairwise regulatory interactions, which are not explicitly captured by motif-induced hypergraphs. This limitation may lead to the omission of essential regulatory information. To allay such deficiencies, we introduce an additional graph convolutional channel to model explicit pairwise dependencies, thereby complementing the higher order features. The final gene embeddings, which integrate both graph convolution and multichannel aggregation, are defined as follows:

$$\begin{aligned}\mathbf{X}_{binary}^{(l+1)} &= \text{ReLU}\left(\tilde{\mathbf{D}}^{-\frac{1}{2}}\tilde{\mathbf{S}}\tilde{\mathbf{D}}^{-\frac{1}{2}}\mathbf{X}_{binary}^{(l)}\mathbf{W}_s^{(l)} + \mathbf{b}^{(l)}\right)\\ \mathbf{X}_{Trans}^{(l+1)} &= \lambda_1\mathbf{X}_{higher}^{(l+1)} + \lambda_2\mathbf{X}_{binary}^{(l+1)}.\end{aligned} \tag{6}$$

Let $\tilde{\mathbf{S}} = \mathbf{S} + \mathbf{I}$ denote the binary regulatory adjacency matrix with self-loops, where $\mathbf{I}$ is the identity matrix, and let $\tilde{\mathbf{D}}$ be its corresponding degree matrix. The symmetrically normalized matrix $\hat{\mathbf{S}} = \tilde{\mathbf{D}}^{-1/2}\tilde{\mathbf{S}}\tilde{\mathbf{D}}^{-1/2}$ is employed for graph convolution. Here, $\mathbf{X}_{binary}^{(l)}$ denotes the input embedding, while $\mathbf{X}_{binary}^{(l+1)}$ is the updated pairwise regulatory representation obtained via the $(l+1)$th GCN layer, with learnable weights $\mathbf{W}_s^{(l)}$ and bias $\mathbf{b}^{(l)}$.

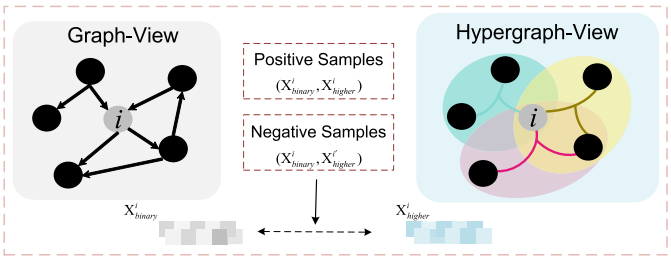

Fig. 4. Cross-view self-supervised contrastive learning.

The activation function ReLU(·) introduces nonlinearity. The final gene embedding $\mathbf{X}_{Trans}^{(l+1)}$ combines higher order semantic features and explicit pairwise interactions, weighted by hyperparameters λ_1 and λ_2, respectively.

D. Regulatory Association Prediction

To quantify regulatory strength, we compute the dot product between gene embeddings, resulting in a score matrix $\mathbf{R} = \text{ReLU}(\mathbf{X}_{Trans}^{(l+1)}(\mathbf{X}_{Trans}^{(l+1)})^\top)$, where $\mathbf{R}(i,j)$ denotes the predicted regulatory score between genes i and j, with higher values indicating stronger associations. Given the original GRN adjacency matrix $\mathbf{S}$ and the reconstructed association matrix $\mathbf{R}$, the loss function for the downstream task is defined as

$$\mathcal{L}_{pri} = \sum_{(i,j)\in\Psi^+\cup\Psi^-}\Phi\left(\mathbf{R}\left(i,\mathrm{j}\right),\mathbf{S}\left(i,j\right)\right) + \delta\left\|\Theta\right\|_{\mathrm{F}}^2 \tag{7}$$

where Ψ^+ and Ψ^- are the sets of positive and negative training pairs, respectively; $\Phi(\cdot)$ denotes the mean squared error (mse) loss between predicted scores and ground-truth labels; δ controls the ℓ_2-regularization strength; and Θ represents the trainable parameters of the Motif-GRN model.

E. Enhancing Motif-GRN via Cross-View Supervision

In our approach, the motif-induced hypergraph channel is designed to capture implicit higher order regulatory semantics, while the GCN-based channel models explicit pairwise gene regulatory interactions. To exploit the potential synergy between these two complementary perspectives, we propose a cross-view self-supervised learning mechanism to enhance gene representations. Specifically, we design a cross-view contrastive learning module (as illustrated in Fig. 4), which encourages consistency between representations derived from the explicit and higher order regulatory views. We adopt InfoNCE as the optimization objective to maximize cross-view alignment. The corresponding loss function is defined as

$$\mathcal{L}_{ssl} = \sum_{i\in G} -\log\frac{\exp\left(S\left(\mathbf{X}_{binary}^i, \mathbf{X}_{higher}^i\right)\Big/\tau\right)}{\sum_{i'=0}^{G}\exp\left(S\left(\mathbf{X}_{binary}^i, \mathbf{X}_{higher}^{i'}\right)\Big/\tau\right)} \tag{8}$$

where,$\mathbf{X}_{binary}^i$ and $\mathbf{X}_{higher}^i$ denote the explicit pairwise regulatory features and motif-induced higher order features of gene i, respectively. The similarity function $S(\cdot,\cdot)$ is instantiated as cosine similarity, and τ is a temperature hyperparameter controlling the sharpness of the distribution. We treat the representations of the same gene across two regulatory views

as a positive pair, and those of different genes within the same mini-batch as negative pairs. Following the contrastive learning paradigm, this objective leverages implicit supervision by distinguishing positive from negative samples to enhance the quality of gene embeddings. Finally, we jointly optimize the primary objective and the auxiliary contrastive loss as

$$\mathcal{L} = \mathcal{L}_{pri} + \beta \mathcal{L}_{ssl}. \tag{9}$$

F. Inductive Motif-Aware Hypergraph Learning for Generalizable GRN Inference

In recent years, supervised approaches for GRN inference have consistently outperformed unsupervised methods. However, the scarcity of reliable regulatory interactions renders real-world GRNs highly sparse, severely hindering the effectiveness of existing computational models in practical settings. Spectral GNNs, bound to predefined Laplacians, are transductive and cannot generalize to unseen structures. In contrast, inductive graph representation learning leverages learnable aggregation functions to capture local neighborhood information, enabling adaptability to dynamic graphs and cross-graph generalization. Therefore, we propose an inductive motif-aware hypergraph learning framework that supports GRN inference across multiple graphs. Specifically, we replace the motif-aware hypergraph convolution operation, originally defined in (4), with a learnable inductive propagation scheme applied to the motif-induced adjacency matrix. By iterative updates of the feature transformation function, the model learns higher order semantic embeddings for genes. The update rule is formally expressed as follows:

$$\mathbf{X}_{t'} = f_{\phi}\left(\mathbf{X}_t, \mathbf{A}_{M_t}\right) \tag{10}$$

where $\mathbf{X}_t$ denotes the initial gene embedding matrix for the tth channel and $\mathbf{A}_{M_t}$ represents the motif-induced hypergraph adjacency matrix corresponding to that channel. The symbol ϕ refers to the trainable parameters of the feature transformation function, and $\mathbf{X}_{t'}$ denotes the resulting gene representations obtained through inductive representation learning. The function $f(\cdot)$ computes attention weights over the neighborhoods of gene nodes in the motif-induced hypergraph using a multihead attention mechanism. These attention weights are then used to aggregate higher order regulatory signals from each node's neighborhood, thereby enhancing the semantic representation of regulatory patterns. The formal computation is defined as follows:

$$\begin{aligned}
\alpha_{vu} &= \frac{\exp\left(\text{LeakyReLU}\left(a^T\left[\mathbf{W}\mathbf{X}_t^v \| \mathbf{W}\mathbf{X}_t^u\right]\right)\right)}{\sum_{u\in\mathcal{N}(v)}\exp\left(\text{LeakyReLU}\left(a^T\left[\mathbf{W}\mathbf{X}_t^v \| \mathbf{W}\mathbf{X}_t^u\right]\right)\right)} \\
\mathbf{X}_{t'}^v &= \Big\|_{k=1}^{3}\sigma\left(\sum_{u\in\mathcal{N}(v)}\alpha_{vu}^k\mathbf{W}^k\mathbf{X}_t^u\right)
\end{aligned} \tag{11}$$

where $\mathbf{W}$ denotes the shared learnable weight matrix for updating gene features, while $\mathbf{X}_t^v$ and $\mathbf{X}_t^u$ represent the input embeddings of gene v and its neighbor u in the tth channel, respectively. The vector $\mathbf{a}$ is a trainable attention vector, $\mathcal{N}(v)$ denotes the higher order implicit regulatory neighbors of gene v sharing the same motif structure, and $\|$ denotes the feature concatenation operator. The multihead attention mechanism adaptively aggregates neighborhood features and computes the updated representation $\mathbf{X}_{t'}^v$ for each gene. After $(l+1)$ layers of propagation, the final higher order representation is obtained by aggregating gene features from ten motif-induced views using the semantic attention mechanism defined in (5), yielding $\mathbf{X}_{higher'}^{(l+1)} = \sum_{t=1}^{10}\alpha_t\mathbf{X}_{t'}^{(l+1)}$, where α_t denotes the attention weight assigned to the tth motif-specific hypergraph channel.

To effectively capture explicit pairwise regulatory relationships within the inductive learning framework, we employ the graph attention network (GAT) [60], a representative inductive graph representation learning method that leverages self-attention mechanisms to dynamically adjust the importance of neighboring nodes and learn expressive feature representations. In contrast to methods relying on static adjacency matrices, GAT offers superior generalization ability, enabling the model to propagate and generate meaningful representations for previously unseen nodes or subgraph structures. This capability substantially enhances the adaptability of the model to new samples and cross-dataset scenarios.

Based on the aforementioned statements, we design a two-layer GAT module, formally defined as

$$\mathbf{X}'_{binary} = \text{GAT}_{\phi^{(2)}}\left(\text{GAT}_{\phi^{(1)}}\left(\mathbf{X},\mathbf{S}\right),\mathbf{S}\right) \tag{12}$$

where $\mathbf{X}$ denotes the input feature matrix, $\mathbf{S}$ is the adjacency matrix representing explicit regulatory interactions, and $\phi^{(1)}$ and $\phi^{(2)}$ are the learnable parameters of the two GAT layers.

Algorithm 1 Motif-GRN Inference Method

Input: Feature matrix $\mathbf{X}$, ground-truth network $\mathbf{S}$
Output: Inferred gene regulatory network $\mathbf{R}$
Compute statistically significant motifs in $\mathbf{S}$
Construct motif-induced hypergraph $\mathcal{G}$
Derive $\mathbf{A}_{M_t}$ from Table I
if Transductive GRN inference, **then**
  $\mathbf{X}_t^{(l+1)} \leftarrow \widehat{\mathbf{D}}_t^{-1}\mathbf{A}_{M_t}\mathbf{X}_t^{(l)}$
  $\alpha_t \leftarrow f_{\text{att}}(\mathbf{X}_t^{(l+1)})$
  $\mathbf{X}_{higher}^{(l+1)} \leftarrow \sum_{t=1}^{10}(\alpha_t\mathbf{X}_t^{(l+1)})$
  $\mathbf{X}_{binary}^{(l+1)} \leftarrow \text{ReLU}\left(\tilde{\mathbf{D}}^{-\frac{1}{2}}\tilde{\mathbf{S}}\tilde{\mathbf{D}}^{-\frac{1}{2}}\mathbf{X}_{binary}^{(l)}\mathbf{W}_s^{(l)} + \mathbf{b}^{(l)}\right)$
  $\mathbf{X}_{Trans}^{(l+1)} \leftarrow \lambda_1\mathbf{X}_{higher}^{(l+1)} + \lambda_2\mathbf{X}_{binary}^{(l+1)}$
  $\mathbf{R} \leftarrow \text{ReLU}(\mathbf{X}_{Trans}^{(l+1)}(\mathbf{X}_{Trans}^{(l+1)})^\top)$
  $\mathcal{L}_{pri} \leftarrow \sum_{(i,j)\in\Psi^+\cup\Psi^-}\Phi(\mathbf{R}(i,j),\mathbf{S}(i,j)) + \delta\|\Theta\|_F^2$
  $\mathcal{L}_{ssl} \leftarrow \sum_{i\in G} -\log\frac{\exp(S(\mathbf{X}_{binary}^i,\mathbf{X}_{higher}^i)/\tau)}{\sum_{i'=0}^{G}\exp(S(\mathbf{X}_{binary}^i,\mathbf{X}_{higher}^{i'})/\tau)}$
  $\mathcal{L} \leftarrow \mathcal{L}_{pri} + \beta\mathcal{L}_{ssl}$
else
  /* Inductive GRN inference */
  $\mathbf{X}_{t'} \leftarrow f_{\phi}(\mathbf{X}_t, \mathbf{A}_{M_t})$
  $\mathbf{X}_{higher'}^{(l+1)} \leftarrow \sum_{t=1}^{10}\alpha_t\mathbf{X}_{t'}^{(l+1)}$
  $\mathbf{X}'_{binary} \leftarrow \text{GAT}_{\phi^{(2)}}(\text{GAT}_{\phi^{(1)}}(\mathbf{X},\mathbf{S}),\mathbf{S})$
  $\mathbf{X}_{Ind}^{(l+1)} \leftarrow \lambda_1\mathbf{X}_{higher'}^{(l+1)} + \lambda_2\mathbf{X}'_{binary}$
  $\mathbf{R} \leftarrow \text{ReLU}(\mathbf{X}_{Ind}^{(l+1)}(\mathbf{X}_{Ind}^{(l+1)})^\top)$
  Repeat steps 13–15 until convergence
end if
return R

By aggregating the explicit pairwise regulatory representation $\mathbf{X}'_{binary}$ and the higher order implicit feature representation $\mathbf{X}^{(l+1)}_{higher'}$, we obtain the final gene representation under the inductive framework as $\mathbf{X}^{(l+1)}_{Ind} = \lambda_1 \mathbf{X}^{(l+1)}_{higher'} + \lambda_2 \mathbf{X}'_{binary}$. Subsequently, the regulatory interaction score matrix is computed by performing an inner product on the TF and target gene representations followed by a ReLU activation, i.e., $\mathbf{R} = \text{ReLU}(\mathbf{X}^{(l+1)}_{Ind} \mathbf{X}^{(l+1)^\top}_{Ind})$. It is worth noting that although the multichannel graph encoders under the inductive and transductive paradigms differ in network structure and optimization schemes, they share the same optimization objectives for both the main gene regulation inference task and the auxiliary self-supervised learning task. Detailed formulations are provided in (7)–(9) and are omitted here for brevity. The Motif-GRN framework is summarized in Algorithm 1.

IV. Experiments

A. Datasets and Data Preprocessing

To assess the performance of Motif-GRN in inferring GRNs, we utilize seven single-cell RNA sequencing (scRNA-seq) datasets from both mouse and human sources. These include mouse dendritic cells (mDCs), embryonic stem cells (mESCs), and hematopoietic stem cells from erythroid (mHSC-E), granulocyte-monocyte (mHSC-GM), and lymphoid-like (mHSC-L) lineages, as well as human embryonic stem cells (hESCs) and mature hepatocytes (hHEP). Following the recommendation in [49], we select TFs with adjusted variance p-value below 0.01, along with the top 500 and 1000 most differentially expressed genes in each dataset. Each scRNA-seq dataset is evaluated against three types of ground-truth regulatory networks: 1) nonspecific ChIP-seq [50]; 2) cell-type-specific ChIP-seq [51]; and 3) STRING functional associations [52]. Detailed statistics for these networks are provided in Supplementary Material, Tables S22–S24. The implemented code of Motif-GRN used in this study is available at https://anonymous.4open.science/r/Motif-GRN-B83E

B. Experimental Setting

We evaluate Motif-GRN on seven benchmark scRNA-seq datasets using three widely recognized ground-truth GRNs: STRING, Nonspecific ChIP-seq, and Cell-type-specific ChIP-seq. To fairly assess generalization under heterogeneous network densities, we adopt a tailored data partitioning strategy.

For the STRING and Nonspecific ChIP-seq networks, two-thirds of known TF–gene pairs are randomly assigned as positive training samples, with the remaining third reserved for testing. All unlabeled TF–gene pairs are treated as candidate negatives. Since the negatives vastly outnumber the positives, we perform uniform random sampling with additional constraints to ensure balanced and fair evaluation. Specifically, during training, each positive-negative pair shares the same TF to maintain regulatory context consistency. During testing, the positive-to-negative ratio is controlled according to the following formula:

$$\frac{Positive}{Negative} = \frac{Network\ Density}{1 - Network\ Density} \tag{13}$$

where *Positive* and *Negative* denote the number of positive and negative samples in the test set, respectively, and *Network Density* refers to the edge density of the ground-truth GRN. The density values for each dataset are summarized in Supplementary Material, Tables S22–S24.

For the cell-type-specific ground-truth networks, due to the relatively small number of active TFs and the high connectivity of these TF nodes, we partition the target (positive) and nontarget (negative) genes into training and testing subsets using a proportional sampling strategy. During training, the Adam optimizer is employed to update the model parameters until convergence. Considering the inherent imbalance between positive and negative samples, we adopt two widely used evaluation metrics, the area under the receiver operating characteristic curve (AUROC) and the area under the precision–recall curve (AUPRC) to comprehensively assess the model's predictive performance.

C. Baseline Methods

Motif-GRN is compared with seven representative supervised and unsupervised methods. All baselines are run with default hyperparameters, and supervised models are trained and tested using the same data splits for fairness. The baseline methods are summarized as follows.

1) GENIE3 [9] treats GRN inference as a feature selection problem, using random forests or gradient boosting to extract regulatory relationships from gene expression data.
2) GENELink [16] integrates prior regulatory evidence with expression profiles and refines gene representations via a GAT, showing strong performance on scRNA-seq data.
3) GNNLink [28] extends GENELink by preprocessing raw scRNA-seq data to enhance regulatory signals, formulating GRN inference as link prediction, and employing GCNs to capture gene dependencies.
4) GRANet [30] is a recent GNN-based method for GRN inference from gene expression data, which models regulatory dependencies via graph representation learning and achieves strong performance on multiple benchmark datasets.
5) GATCL [55] is a graph attention-based approach for GRN inference from single-cell RNA-seq data, leveraging attention mechanisms to aggregate regulatory signals and serving as a competitive recent baseline for GRN reconstruction.
6) GNE [56] leverages deep learning to fuse gene expression and interaction networks, learning low-dimensional gene embeddings for improved interaction prediction.
7) DeepSEM [57] is a deep generative model based on structural equation modeling that captures gene regulatory dependencies through neural network constraints.
8) GRN-Transformer [58] uses axial Transformers in a weakly supervised framework to infer cell-type-specific GRNs by integrating bulk and single-cell RNA-seq data.
9) DeepDRIM [59] converts joint gene expression into 2-D histograms and incorporates neighborhood context,

TABLE II

AUROC SCORES OF DIFFERENT METHODS ON VARIOUS DATASETS UNDER TFS+ 500 AND TFS+ 1000 SETTINGS

Datasets	Cell Type	TFs+500										TFs+1000									
		Motif-GRN	GRANet	GATCL	GNNLink	GENELink	GNE	DeepSEM	GRN-Transformer	DeepDRIM	GENIE3	Motif-GRN	GRANet	GATCL	GNNLink	GENELink	GNE	DeepSEM	GRN-Transformer	DeepDRIM	GENIE3
STRING	hESC	**0.95**	0.90	0.90	0.92	0.88	0.73	0.60	0.62	0.61	0.34	**0.94**	0.92	0.91	0.91	0.88	0.75	0.63	0.61	0.58	0.64
	hHEP	**0.93**	0.92	0.91	0.89	0.87	0.73	0.61	0.61	0.52	0.54	**0.93**	0.92	0.92	0.88	0.90	0.75	0.61	0.58	0.47	0.63
	mDC	**0.94**	0.92	0.90	0.92	0.88	0.76	0.57	0.61	0.57	0.50	**0.95**	0.92	0.90	0.91	0.88	0.78	0.57	0.43	0.47	0.60
	mESC	**0.94**	0.93	0.92	0.91	0.88	0.76	0.60	0.60	0.58	0.50	**0.95**	0.93	0.92	0.90	0.88	0.79	0.60	0.56	0.64	0.61
	mHSC-E	**0.94**	0.89	0.92	0.91	0.89	0.63	0.68	0.66	0.42	0.52	**0.94**	0.90	0.91	0.90	0.89	0.65	0.65	0.61	0.60	0.70
	mHSC-GM	**0.94**	0.87	0.89	0.92	0.87	0.69	0.72	0.64	0.58	0.53	**0.93**	0.87	0.88	0.91	0.82	0.69	0.69	0.58	0.61	0.75
	mHSC-L	**0.89**	0.82	0.79	0.83	0.75	0.72	0.67	0.63	0.64	0.52	**0.90**	0.82	0.74	0.86	0.72	0.71	0.68	0.72	0.76	0.71
Non-specific ChIP-seq	hESC	**0.87**	0.72	0.75	0.80	0.69	0.63	0.53	0.47	0.48	0.45	**0.90**	0.75	0.77	0.81	0.69	0.63	0.53	0.61	0.58	0.45
	hHEP	**0.88**	0.74	0.76	0.83	0.70	0.63	0.54	0.48	0.45	0.45	**0.90**	0.83	0.82	0.84	0.71	0.62	0.55	0.58	0.45	0.45
	mDC	**0.87**	0.85	0.86	0.86	0.80	0.67	0.57	0.52	0.58	0.55	**0.89**	0.85	0.86	0.86	0.79	0.67	0.56	0.45	0.45	0.52
	mESC	**0.86**	0.80	0.81	0.84	0.75	0.67	0.56	0.58	0.59	0.56	**0.88**	0.82	0.83	0.86	0.76	0.69	0.56	0.56	0.63	0.56
	mHSC-E	**0.87**	0.74	0.78	0.84	0.76	0.56	0.61	0.59	0.54	0.64	**0.89**	0.78	0.82	0.83	0.76	0.56	0.59	0.61	0.60	0.63
	mHSC-GM	**0.89**	0.79	0.77	0.80	0.70	0.60	0.65	0.61	0.75	0.71	**0.92**	0.80	0.81	0.85	0.73	0.62	0.61	0.58	0.61	0.70
	mHSC-L	**0.85**	0.64	0.57	0.71	0.66	0.60	0.59	0.65	0.61	0.65	**0.84**	0.78	0.73	0.76	0.60	0.59	0.60	0.72	0.75	0.65
Cell-type-specific ChIP-seq	hESC	**0.86**	0.85	0.86	0.83	0.83	0.67	0.58	0.51	0.48	0.49	**0.87**	0.86	0.86	0.84	0.84	0.68	0.58	0.67	0.56	0.45
	hHEP	**0.88**	0.87	0.85	0.82	0.83	0.80	0.55	0.48	0.52	0.54	**0.89**	0.88	0.86	0.82	0.83	0.81	0.55	0.57	0.63	0.54
	mDC	**0.74**	0.73	0.74	0.66	0.68	0.52	0.51	0.48	0.48	0.49	**0.77**	0.75	0.75	0.72	0.73	0.52	0.51	0.45	0.45	0.52
	mESC	**0.93**	0.90	0.89	0.82	0.88	0.81	0.50	0.53	0.51	0.50	**0.94**	0.94	0.90	0.82	0.86	0.82	0.50	0.59	0.62	0.46
	mHSC-E	**0.90**	0.87	0.84	0.80	0.86	0.82	0.51	0.64	0.56	0.52	**0.92**	0.90	0.89	0.82	0.90	0.84	0.51	0.53	0.46	0.50
	mHSC-GM	**0.91**	0.90	0.89	0.86	0.89	0.83	0.53	0.49	0.64	0.53	**0.93**	0.92	0.84	0.86	0.90	0.84	0.53	0.58	0.66	0.51
	mHSC-L	**0.87**	0.84	0.83	0.83	0.82	0.77	0.54	0.64	0.58	0.52	**0.88**	0.86	0.83	0.84	0.84	0.77	0.54	0.42	0.57	0.52

The best results are highlighted in **bold**, and the second-best results are underlined.

TABLE III

AUPRC SCORES OF DIFFERENT METHODS ON VARIOUS DATASETS UNDER TFS+ 500 AND TFS+ 1000 SETTINGS

Datasets	Cell Type	TFs+500										TFs+1000									
		Motif-GRN	GRANet	GATCL	GNNLink	GENELink	GNE	DeepSEM	GRN-Transformer	DeepDRIM	GENIE3	Motif-GRN	GRANet	GATCL	GNNLink	GENELink	GNE	DeepSEM	GRN-Transformer	DeepDRIM	GENIE3
STRING	hESC	0.40	0.35	0.30	**0.43**	0.16	0.05	0.05	0.03	0.04	0.04	**0.40**	0.32	0.30	0.30	0.13	0.05	0.05	0.03	0.05	0.03
	hHEP	0.36	**0.37**	0.27	0.28	0.21	0.05	0.05	0.06	0.05	0.06	**0.34**	0.30	0.31	0.26	0.23	0.05	0.05	0.06	0.03	0.02
	mDC	**0.50**	0.43	0.31	0.42	0.29	0.09	0.07	0.04	0.04	0.05	**0.49**	0.42	0.25	0.41	0.28	0.09	0.07	0.04	0.05	0.06
	mESC	**0.37**	0.34	0.28	0.27	0.15	0.05	0.05	0.04	0.05	0.04	**0.40**	0.39	0.26	0.25	0.13	0.05	0.05	0.04	0.05	0.02
	mHSC-E	0.40	0.37	0.37	0.36	0.23	0.04	0.16	0.12	0.09	0.12	**0.47**	0.38	0.39	0.36	0.18	0.04	0.16	0.12	0.13	0.12
	mHSC-GM	**0.59**	0.42	0.39	0.50	0.22	0.07	0.28	0.27	0.26	0.27	**0.52**	0.39	0.43	0.38	0.14	0.07	0.28	0.27	0.26	0.25
	mHSC-L	**0.63**	0.35	0.34	0.56	0.23	0.09	0.32	0.29	0.32	0.33	**0.57**	0.35	0.33	0.56	0.24	0.09	0.32	0.29	0.30	0.32
Non-specific ChIP-seq	hESC	**0.15**	0.06	0.05	0.09	0.04	0.02	0.02	0.02	0.02	0.02	**0.15**	0.067	0.10	0.08	0.04	0.02	0.02	0.02	0.02	0.01
	hHEP	**0.15**	0.08	0.08	0.10	0.05	0.02	0.02	0.01	0.02	0.02	**0.18**	0.13	0.079	0.11	0.05	0.02	0.02	0.01	0.02	0.01
	mDC	**0.23**	0.22	0.19	0.21	0.17	0.03	0.04	0.02	0.02	0.02	**0.23**	0.22	0.18	0.21	0.12	0.02	0.03	0.02	0.03	0.02
	mESC	**0.13**	0.13	0.097	0.11	0.04	0.02	0.02	0.02	0.02	0.02	**0.14**	0.11	0.073	0.12	0.04	0.02	0.02	0.02	0.02	0.02
	mHSC-E	0.20	**0.21**	0.19	0.19	0.10	0.03	0.08	0.05	0.05	0.06	0.22	0.16	**0.26**	0.17	0.11	0.02	0.07	0.05	0.06	0.05
	mHSC-GM	**0.28**	0.22	0.24	0.21	0.16	0.04	0.12	0.12	0.12	0.12	**0.35**	0.23	0.25	0.27	0.24	0.04	0.11	0.12	0.15	0.12
	mHSC-L	**0.28**	0.12	0.14	0.20	0.13	0.06	0.13	0.11	0.09	0.13	**0.19**	0.18	0.17	0.19	0.10	0.05	0.13	0.14	0.13	0.12
Cell-type-specific ChIP-seq	hESC	0.53	**0.58**	0.56	0.49	0.48	0.34	0.19	0.15	0.13	0.15	0.55	**0.60**	0.57	0.50	0.52	0.34	0.19	0.16	0.19	0.15
	hHEP	0.78	**0.81**	0.72	0.67	0.68	0.65	0.40	0.35	0.39	0.39	0.77	**0.81**	0.73	0.66	0.69	0.66	0.41	0.53	0.46	0.38
	mDC	**0.13**	0.12	0.11	0.13	0.10	0.06	0.05	0.06	0.06	0.05	**0.17**	0.13	0.12	0.14	0.11	0.05	0.05	0.05	0.06	0.05
	mESC	0.75	**0.82**	0.74	0.62	0.73	0.64	0.31	0.49	0.46	0.31	0.75	**0.86**	0.72	0.60	0.70	0.65	0.31	0.51	0.46	0.31
	mHSC-E	**0.91**	0.85	0.81	0.80	0.88	0.80	0.56	0.71	0.76	0.56	**0.92**	0.91	0.86	0.80	0.91	0.81	0.56	0.69	0.73	0.54
	mHSC-GM	**0.91**	0.90	0.86	0.83	0.90	0.78	0.52	0.66	0.64	0.53	**0.93**	0.92	0.84	0.85	0.91	0.81	0.54	0.61	0.64	0.53
	mHSC-L	**0.85**	0.82	0.81	0.79	0.80	0.70	0.53	0.64	0.59	0.50	**0.85**	0.83	0.80	0.79	0.82	0.68	0.52	0.52	0.48	0.48

The best results are highlighted in **bold**, and the second-best results are underlined.

combining local and global features to improve regulatory interaction prediction.

D. Performance on Benchmark Datasets

We evaluate the performance of Motif-GRN on seven scRNA-seq benchmark datasets under three widely used ground-truth regulatory networks, including STRING, Non-specific ChIP-seq, and Cell-type-specific ChIP-seq. AUROC and AUPRC are adopted as the primary evaluation metrics, and comparisons are conducted against nine representative baseline methods, including two recently proposed graph-based GRN inference approaches, GRANet and GATCL.

As reported in Table II, Motif-GRN consistently achieves the best AUROC performance across almost all datasets and experimental settings, as indicated by the boldface entries. Importantly, in the few cases where Motif-GRN is not ranked first, it is consistently identified as the second-best method, highlighted by underlined results, and no baseline method demonstrates a clear performance advantage over Motif-GRN. This pattern holds across all three ground-truth regulatory networks, including STRING, Nonspecific ChIP-seq, and Cell-type-specific ChIP-seq, demonstrating the stability and robustness of Motif-GRN under diverse regulatory contexts. Notably, even when compared with strong recent baselines such as GRANet and GATCL, Motif-GRN maintains a consistently top-ranked position, reflecting its superior capability in capturing global regulatory relationships.

Given the severe class imbalance and sparsity inherent in GRNs, AUROC alone may not fully reflect model performance under highly skewed label distributions. We therefore further report AUPRC results in Table III as a complementary evaluation metric, where the best and second-best performances are also explicitly indicated. As shown, Motif-GRN is predominantly ranked first in terms of AUPRC across all benchmark datasets and remains consistently within the top two methods in all remaining cases. Under the STRING and Nonspecific ChIP-seq settings, Motif-GRN exhibits clear advantages over competitive baselines, including GRANet, GATCL, and GNNLink. Moreover, under the Cell-type-specific ChIP-seq ground-truth networks, Motif-GRN demonstrates stable precision–recall performance across diverse cell types, further confirming its effectiveness in reconstructing highly sparse and cell-type-dependent regulatory structures.

TABLE IV

AUPRC OF GENIE3 AND DEEPSEM FOR GRN INFERENCE USING SIGNIFICANTLY ALTERED TFS AND THE TOP 500 (LEFT) AND 1000 (RIGHT) EXPRESSED GENES PER DATASET

Cell types	STRING		Non-Specific		Cell-type-Specific	
	GENIE3	DeepSEM	GENIE3	DeepSEM	GENIE3	DeepSEM
mHSC-L	0.52 (0.71)	0.67 (0.68)	0.65 (0.65)	0.59 (0.65)	0.52 (0.52)	0.54 (0.54)
mHSC-GM	0.53 (0.75)	0.72 (0.69)	0.71 (0.77)	0.65 (0.61)	0.53 (0.51)	0.53 (0.53)
mHSC-E	0.52 (0.71)	0.68 (0.65)	0.64 (0.63)	0.61 (0.59)	0.52 (0.52)	0.51 (0.51)
mESC	0.60 (0.66)	0.66 (0.70)	0.65 (0.60)	0.66 (0.56)	0.50 (0.46)	0.50 (0.50)
mDC	0.50 (0.60)	0.57 (0.57)	0.55 (0.52)	0.57 (0.56)	0.49 (0.52)	0.51 (0.51)
hHEP	0.54 (0.63)	0.61 (0.61)	0.45 (0.45)	0.54 (0.55)	0.54 (0.54)	0.55 (0.55)
hESC	0.34 (0.64)	0.60 (0.63)	0.45 (0.45)	0.53 (0.53)	0.49 (0.45)	0.58 (0.58)

TABLE V

AUPRC OF GENIE3 AND DEEPSEM FOR GRN INFERENCE USING SIGNIFICANTLY ALTERED TFS AND THE TOP 500 (LEFT) AND 1000 (RIGHT) EXPRESSED GENES PER DATASET

Cell types	STRING		Non-Specific		Cell-type-Specific	
	GENIE3	DeepSEM	GENIE3	DeepSEM	GENIE3	DeepSEM
mHSC-L	0.33 (0.04)	0.32 (0.32)	0.13 (0.12)	0.13 (0.13)	0.50 (0.48)	0.53 (0.52)
mHSC-GM	0.27 (0.25)	0.26 (0.28)	0.12 (0.12)	0.11 (0.12)	0.52 (0.54)	0.52 (0.54)
mHSC-E	0.12 (0.12)	0.09 (0.16)	0.08 (0.07)	0.09 (0.09)	0.54 (0.62)	0.56 (0.56)
mESC	0.04 (0.02)	0.09 (0.05)	0.10 (0.02)	0.02 (0.02)	0.31 (0.31)	0.31 (0.31)
mDC	0.05 (0.06)	0.04 (0.07)	0.05 (0.04)	0.05 (0.05)	0.35 (0.05)	0.35 (0.05)
hHEP	0.06 (0.02)	0.05 (0.02)	0.05 (0.02)	0.05 (0.03)	0.39 (0.36)	0.40 (0.41)
hESC	0.04 (0.03)	0.04 (0.05)	0.02 (0.01)	0.02 (0.02)	0.15 (0.15)	0.19 (0.19)

Overall, the consistently top-ranked performance of Motif-GRN across both AUROC and AUPRC metrics demonstrates its robustness and reliability across heterogeneous datasets, highlighting the effectiveness of motif-aware modeling in capturing higher order regulatory patterns.

E. Evaluating the Inductive Learning Capabilities of Motif-GRN

Building upon Motif-GRN, we further design and implement a motif-aware hypergraph encoder that supports inductive learning, aiming to enhance the model's generalization ability across datasets and species. To systematically evaluate its inductive inference performance, we conduct cross-dataset experiments on multiple scRNA-seq datasets that shared ground-truth regulatory networks. Specifically, we select one dataset for training and evaluate the model on all related datasets, including the training one, to assess its adaptability to unseen data. AUROC and AUPRC are used as the primary evaluation metrics, and comprehensive assessments are performed under ground-truth networks constructed from STRING and cell-type-specific ChIP-seq data.

To further validate the model's performance, we compare Motif-GRN with the classical unsupervised method GENIE3 [56] and a recent representative method DeepSEM [52]. All methods are evaluated under identical data configurations to ensure fair comparison. The performance of the baseline methods is summarized in Tables IV and V, while the results of Motif-GRN are presented in Supplementary Material, Figs. S3–S10. Together, they form a complete evaluation framework. The results show that Motif-GRN consistently outperforms the competing methods across multiple datasets under the same ground-truth networks, demonstrating its stable and superior inductive inference capability.

Furthermore, to assess the model's inductive capability in cross-species scenarios, we select the STRING TF+ 1000 genes dataset (including mESC and hHEP), which has shown strong performance in prior experiments, as the training set for parameter optimization. Subsequently, we conduct comprehensive evaluations on all relevant scRNA-seq datasets using the ground-truth network constructed from nonspecific ChIP-seq data and repeat the inductive experiments within this network to enable direct comparison. As illustrated in Fig. 5, the model trained on the STRING TF+ 1000 genes dataset consistently achieves top performance across most experimental settings and maintains high stability across datasets. These results suggest that Motif-GRN effectively leverages training data enriched with prior regulatory knowledge and generalizes well to inference tasks in sparse or heterogeneous conditions, thereby enabling robust inductive gene regulatory inference across datasets and species.

F. Ablation Analysis of Multichannel Graph Coding Layers

In order to evaluate the contribution of each core component in the multichannel encoder of Motif-GRN, we construct two simplified variants for ablation experiments. The first variant, Motif-GRN$_{\text{Hyper}}$, retains only the motif-aware hypergraph convolution encoder and removes the base graph convolution encoder. The second variant, Motif-GRN$_{\text{Base}}$, keeps only the base graph convolution encoder while excluding the motif-aware hypergraph component. These variants are evaluated across multiple scRNA-seq datasets with three types of ground-truth networks: STRING, Nonspecific ChIP sequencing, and Cell-type-specific ChIP sequencing. The results on the STRING and Nonspecific ChIP sequencing datasets are presented in Fig. 6 and 7, respectively, while the results for Cell-type-specific ChIP sequencing are provided in Supplementary Material, Fig. S11. All ablation results are reported as the mean $\pm$ standard deviation over five independent runs, and statistical significance is assessed using paired tests.

The experimental results (see Fig. 6 and 7) demonstrate that Motif-GRN, which integrates both the base graph convolution encoder and the motif-aware hypergraph encoder, consistently achieves superior predictive performance across all evaluated datasets. This confirms the effectiveness of jointly modeling both pairwise regulatory dependencies and higher order semantic regulatory patterns. Moreover, Fig. 6 shows that Motif-GRN$_{\text{Hyper}}$, which employs only the motif-aware hypergraph encoder, generally outperforms Motif-GRN$_{\text{Base}}$ in inferring regulatory interactions, highlighting the importance of higher order motif structures. However, the results in Fig. 7 indicate that in certain datasets, the base graph convolution encoder contributes more significantly. This may be attributed to a lower prevalence of higher order regulatory motifs in these datasets, which limits the representational capacity of the hypergraph encoder when used in isolation. These findings further support the necessity of incorporating the base encoder to effectively capture direct pairwise regulatory relationships.

G. Ablation Analysis of the Effectiveness of Self-Supervised Learning

To evaluate the effectiveness of the self-supervised auxiliary task in Motif-GRN, we conduct ablation experiments on the STRING dataset using AUROC and AUPRC as evaluation

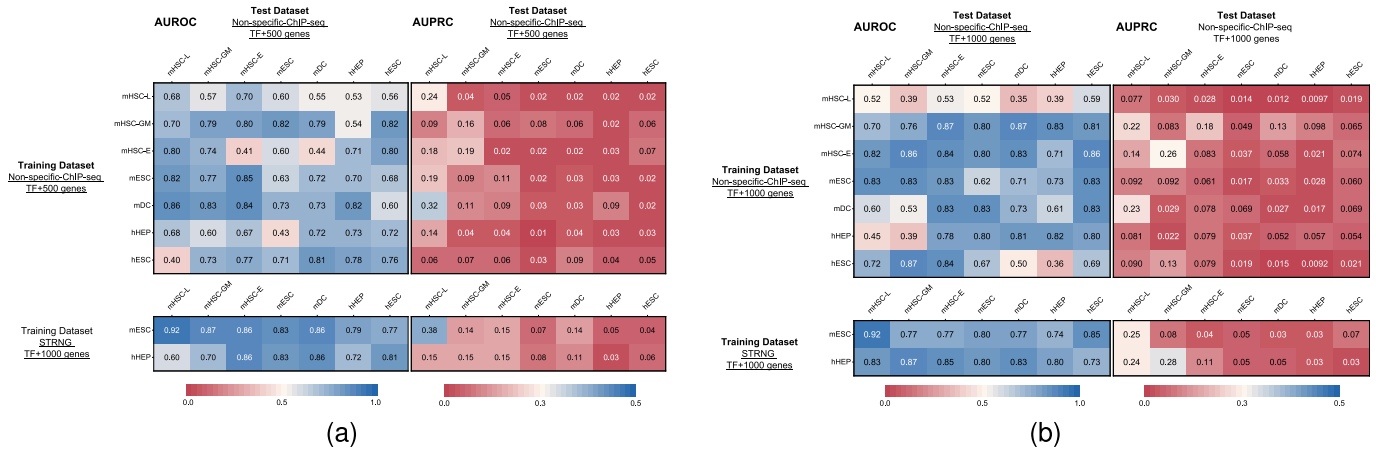

Fig. 5. Inductive inference performance of Motif-GRN based on AUROC and AUPRC. (a) Model is trained on Nonspecific ChIP-seq TF+500 genes and STRING TF+1000 genes. (b) On nonspecific ChIP-seq TF+1000 genes and STRING TF+1000 genes. In both settings, STRING networks are derived from mESC and hHEP, and evaluation is performed on all scRNA-seq datasets associated with the corresponding ChIP-seq configuration.

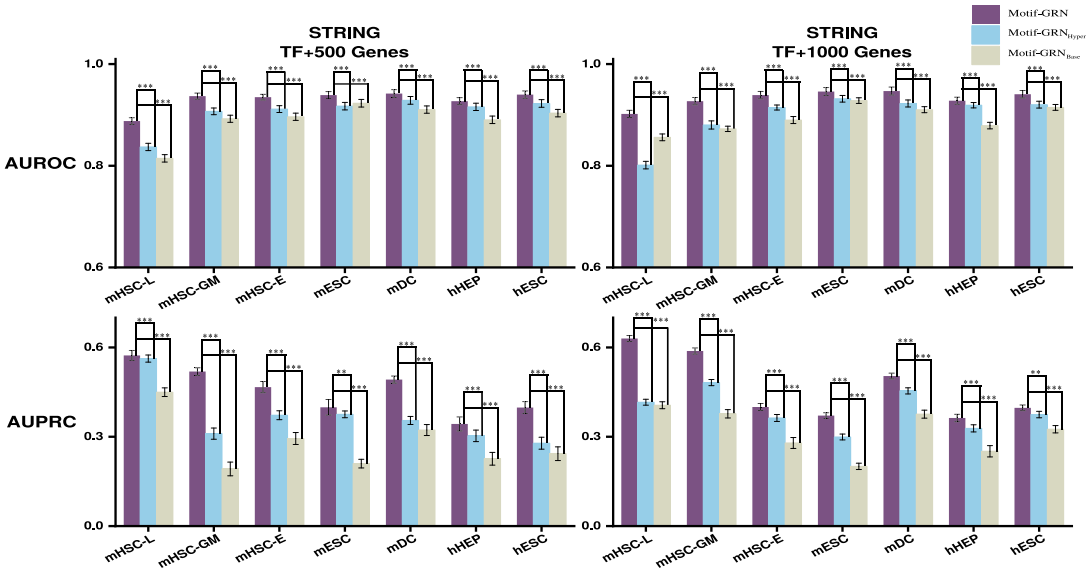

Fig. 6. Ablation study results on the STRING dataset. The upper and lower panels show performance evaluated by AUROC and AUPRC, respectively. Motif-GRN incorporates both the multichannel motif-aware hypergraph encoder and the base graph convolution encoder. Motif-GRN $_{\text{Hyper}}$ retains only the hypergraph encoder, while Motif-GRN$_{\text{Base}}$ includes only the base encoder. All results are reported as the mean $\pm$ standard deviation over five independent runs. Statistical significance between the full model and each ablated variant is assessed using paired statistical tests, with significance levels denoted as follows: *** indicates $p < 1 \times 10^{-3}$, ** indicates $p < 1 \times 10^{-2}$, and * indicates $p < 5 \times 10^{-2}$.

metrics (see Fig. 8). Motif-GRN integrates self-supervised learning signals from both the motif-induced hypergraph view and the standard graph view, and employs a joint optimization strategy to enhance overall performance. In contrast, the ablated variant Motif-GRN* removes the cross-view contrastive learning component, directly aggregating higher order cooperative regulatory features from the motif-induced hypergraph and pairwise features from the base graph encoder for downstream GRN inference.

Experimental results show that incorporating self-supervised learning consistently improves prediction performance across all datasets, demonstrating the effectiveness of contrastive learning for GRN reconstruction. In particular, the cross-view contrastive task facilitates information exchange between the relatively independent higher order and pairwise views, revealing latent regulatory correlations. By maximizing the mutual information across these views, the model learns more expressive gene representations that capture both local and global regulatory patterns, thereby improving inference accuracy. Results on the Cell-type-specific ChIP-seq and Nonspecific ChIP-seq datasets are provided in Supplementary Material, Figs. S12 and S13.

H. Hyperparameter Sensitivity Analysis

To further evaluate the robustness of Motif-GRN with respect to key hyperparameters, we conduct a sensitivity analysis focusing on parameters that have a direct and interpretable impact on model behavior, including the network depth and the temperature parameter τ used in cross-view contrastive learning. All sensitivity experiments are conducted on the cell-type-specific ChIP-seq dataset with TF+500 genes, which serves as a representative benchmark in our study.

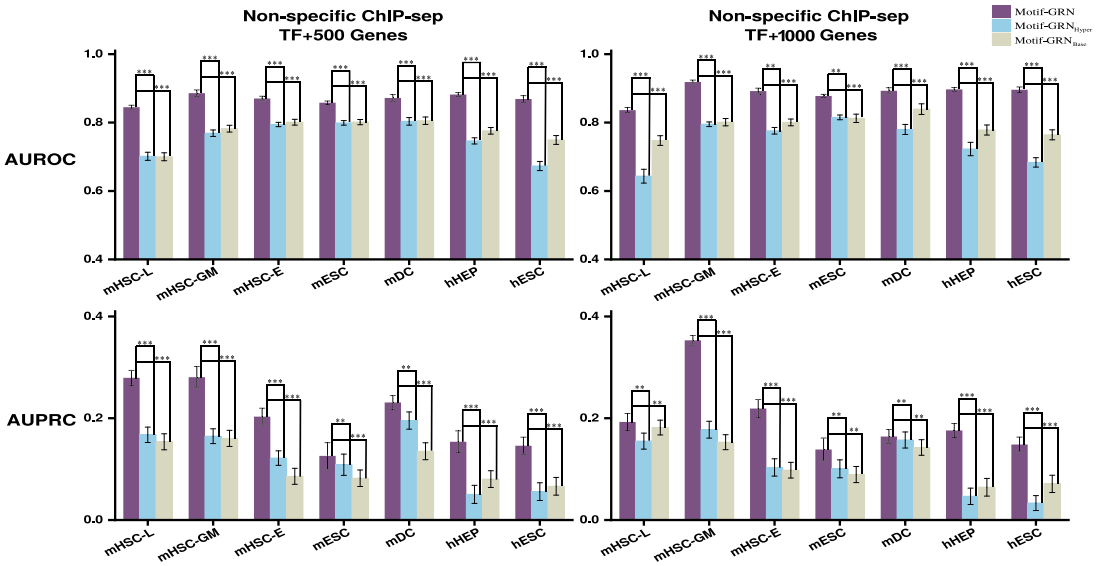

Fig. 7. Ablation study results on the Nonspecific ChIP-seq dataset. The upper and lower panels present performance in terms of AUROC and AUPRC, respectively. The full Motif-GRN model integrates both the multichannel motif-aware hypergraph convolution encoder and the base graph convolution encoder. Motif-GRN $_{\text{Hyper}}$ includes only the motif-aware hypergraph encoder, while Motif-GRN$_{\text{Base}}$ retains only the base graph convolution encoder. All results are reported as the mean $\pm$ standard deviation over five independent runs. Statistical significance between the full model and each ablated variant is assessed using paired statistical tests, with significance levels denoted as follows: *** indicates $p < 1 \times 10^{-3}$, ** indicates $p < 1 \times 10^{-2}$, and * indicates $p < 5 \times 10^{-2}$.

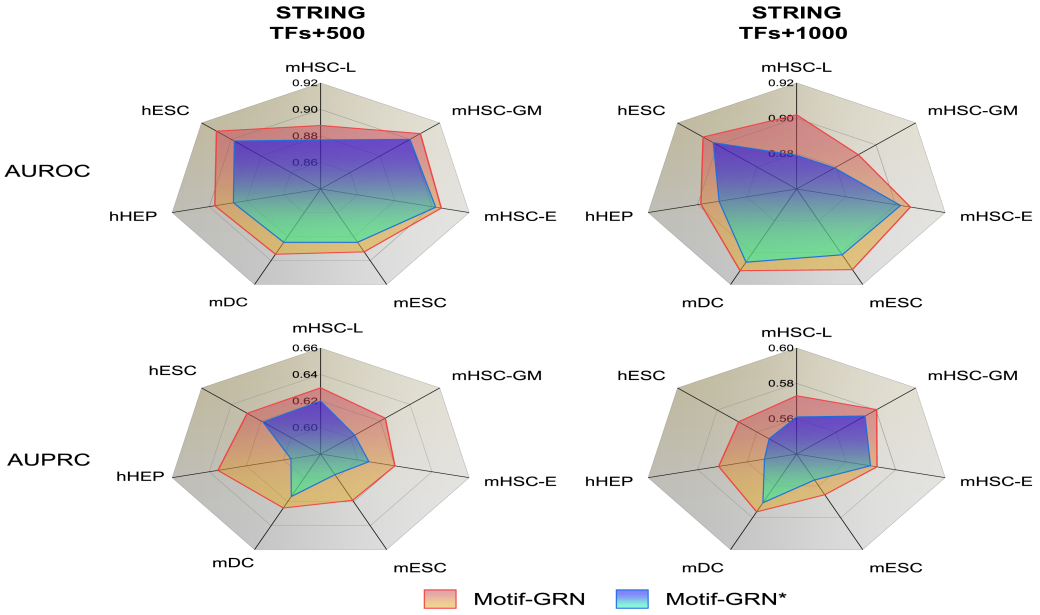

Fig. 8. Ablation study of the self-supervised learning strategy on the STRING dataset. The top panel shows AUROC results, and the bottom panel shows AUPRC results. Motif-GRN integrates a self-supervised learning strategy with joint optimization of primary and auxiliary tasks to enhance GRN inference, whereas Motif-GRN* denotes the ablated model without the self-supervised module.

1) Effect of Network Depth: We first investigate the influence of the number of encoder layers on model performance. Specifically, we vary the depth of the hypergraph and graph encoders from one to five layers while keeping other settings fixed. As shown in Fig. 9(a), increasing the network depth from one to two layers leads to a clear improvement in both AUROC and AUPRC across different cell types. When the depth is further increased beyond two or three layers, the performance tends to saturate or gradually degrade, which is consistent with common observations in graph-based models due to over-smoothing and optimization instability. Based on this analysis, we set the network depth to two layers in all experiments, which provides a favorable balance between model expressiveness, stability, and computational efficiency.

2) Effect of Temperature Parameter τ: We further analyze the sensitivity of Motif-GRN to the temperature parameter τ in the cross-view contrastive learning objective. Fig. 9(b) illustrates the performance variation under different τ values. The results indicate that Motif-GRN maintains relatively stable AUROC and AUPRC performance over a broad range of τ, suggesting that the proposed cross-view supervision mechanism is robust to temperature selection. Rather than selecting

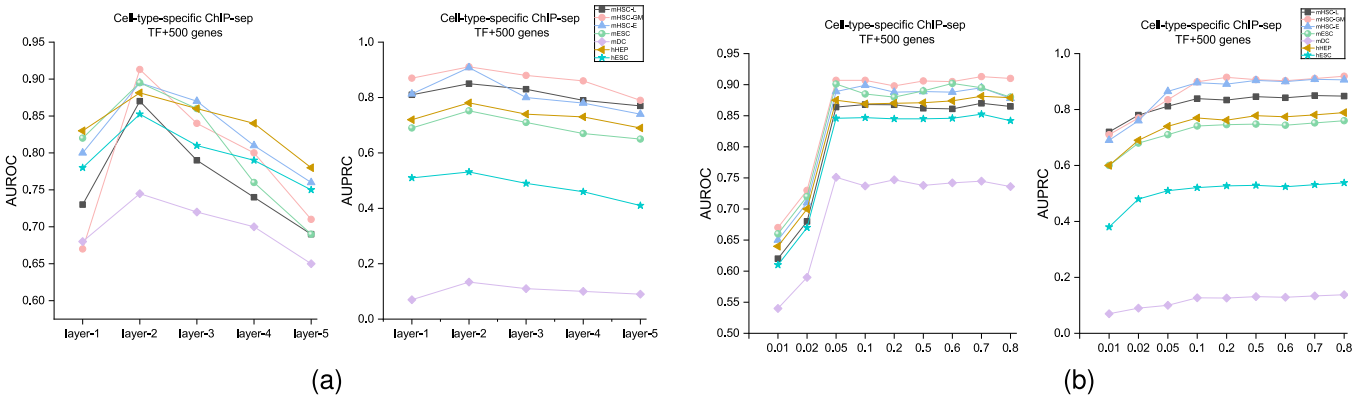

Fig. 9. Sensitivity analysis on the cell-type-specific ChIP-seq dataset (TF+500 genes). (a) Influence of network depth on AUROC and AUPRC across multiple cell types. (b) Influence of the temperature parameter τ in cross-view contrastive learning.

τ based on a single peak value, we choose $\tau = 0.7$ as a representative setting within this stable region, which consistently yields reliable performance across different datasets and cell types. Performance degradation is only observed when τ becomes extremely small or large, which aligns with established findings in contrastive learning literature.

Overall, these analyses demonstrate that Motif-GRN exhibits good robustness to key hyperparameters and that the default configurations adopted in our experiments lie within stable and well-performing regions, supporting the reliability and practical applicability of the proposed framework.

V. Discussion and Conclusion

To explore transcriptional regulatory mechanisms, researchers commonly infer regulatory relationships from gene expression profiles. With the accumulation of prior gene association knowledge, graph-based supervised deep learning approaches have achieved substantial progress in predicting regulatory interactions. However, transcriptional regulation is inherently a complex, multigene cooperative process, and most studies emphasize pairwise relationships between TFs and target genes, overlooking the higher order regulatory patterns pervasive in biological systems, thereby limiting a comprehensive understanding of GRNs. In response, we propose Motif-GRN, a motif-driven hypergraph learning framework for GRN reconstruction. Motif-GRN constructs a multichannel hypergraph from statistically significant three-node motifs, integrates higher order and pairwise regulatory information through a motif-aware hypergraph convolution and a graph convolutional network, and employs cross-view contrastive learning to enhance representation capability. Although higher order motifs with larger sizes (e.g., four-node motifs) may encode more complex regulatory patterns, our systematic statistical analysis demonstrates that most four-node motifs lack stable and consistent enrichment across datasets, which limits their suitability as general-purpose higher order modeling units under the current setting. An inductive extension further enables cross-species and cross-dataset inference, alleviating the challenge of limited prior gene association knowledge in many organisms. Extensive experiments on real-world datasets demonstrate that Motif-GRN effectively captures rich higher order semantic regulatory features and achieves superior performance in both transductive and inductive GRN inference. Despite these promising results, opportunities remain for improvement. While higher order motifs beyond three nodes may be functionally relevant in specific biological contexts, their strong dataset dependence and limited statistical robustness pose challenges for unified modeling, motivating future exploration under more scalable and context-aware frameworks. Future work may integrate multiomics fusion with higher order GNNs to capture complex cross-modal interactions and combine them with dynamic causal inference to better model the temporal evolution of GRNs.

References

[1] F. W. Albert and L. Kruglyak, "The role of regulatory variation in complex traits and disease," *Nature Rev. Genet.*, vol. 16, no. 4, pp. 197–212, Apr. 2015.

[2] G. Karlebach and R. Shamir, "Modelling and analysis of gene regulatory networks," *Nature Rev. Mol. Cell Biol.*, vol. 9, no. 10, pp. 770–780, Oct. 2008.

[3] Y. Qian and S.-S.-C. Huang, "Improving plant gene regulatory network inference by integrative analysis of multi-omics and high resolution data sets," *Current Opinion Syst. Biol.*, vol. 22, pp. 8–15, Aug. 2020.

[4] A. Colaprico et al., "Interpreting pathways to discover cancer driver genes with moonlight," *Nature Commun.*, vol. 11, no. 1, p. 69, Jan. 2020.

[5] C. C. Robertson et al., "Fine-mapping, trans-ancestral and genomic analyses identify causal variants, cells, genes and drug targets for type 1 diabetes," *Nature Genet.*, vol. 53, no. 7, pp. 962–971, Jul. 2021.

[6] Y. You et al., "Artificial intelligence in cancer target identification and drug discovery," *Signal Transduction Targeted Therapy*, vol. 7, no. 1, p. 156, May 2022.

[7] S. Zhou et al., "Single-cell RNA-seq dissects the intratumoral heterogeneity of triple-negative breast cancer based on gene regulatory networks," *Mol. Therapy Nucleic Acids*, vol. 23, pp. 682–690, Mar. 2021.

[8] J. T. Walker et al., "Genetic risk converges on regulatory networks mediating early type 2 diabetes," *Nature*, vol. 624, no. 7992, pp. 621–629, Dec. 2023.

[9] V. A. Huynh-Thu, A. Irrthum, L. Wehenkel, and P. Geurts, "Inferring regulatory networks from expression data using tree-based methods," *PLoS ONE*, vol. 5, no. 9, Sep. 2010, Art. no. e12776.

[10] N. Papili Gao, S. M. M. Ud-Dean, O. Gandrillon, and R. Gunawan, "SINCERITIES: Inferring gene regulatory networks from time-stamped single-cell transcriptional expression profiles," *Nature Commun.*, vol. 9, no. 1, pp. 1–11, 2018.

[11] Z. Li, J. S. Nagai, C. Kuppe, R. Kramann, and I. G. Costa, "ScMEGA: Single-cell multi-omic enhancer-based gene regulatory network inference," *Bioinf. Adv.*, vol. 3, no. 1, Jan. 2023, Art. no. vbad003.

[12] Y. Jiang, Y. Harigaya, Z. Zhang, H. Zhang, C. Zang, and N. R. Zhang, "Nonparametric single-cell multiomic characterization of trio relationships between transcription factors, target genes, and cis-regulatory regions," *Cell Syst.*, vol. 13, no. 9, pp. 737–751, Sep. 2022.

[13] Y. Yuan and Z. Bar-Joseph, "Deep learning for inferring gene relationships from single-cell expression data," *Proc. Nat. Acad. Sci. USA*, vol. 116, no. 52, pp. 27151–27158, Dec. 2019.

[14] Z. Gao, J. Tang, J. Xia, C.-H. Zheng, and P.-J. Wei, "CNNGRN: A convolutional neural network-based method for gene regulatory network inference from bulk time-series expression data," *IEEE/ACM Trans. Comput. Biol. Bioinf.*, vol. 20, no. 5, pp. 2853–2861, Sep. 2023.

[15] J. Wang, A. Ma, Q. Ma, D. Xu, and T. Joshi, "Inductive inference of gene regulatory network using supervised and semi-supervised graph neural networks," *Comput. Struct. Biotechnol. J.*, vol. 18, pp. 3335–3343, Jun. 2020.

[16] G. Chen and Z.-P. Liu, "Graph attention network for link prediction of gene regulations from single-cell RNA-sequencing data," *Bioinformatics*, vol. 38, no. 19, pp. 4522–4529, Sep. 2022.

[17] S. S. Shen-Orr, R. Milo, S. Mangan, and U. Alon, "Network motifs in the transcriptional regulation network of Escherichia coli," *Nature Genet.*, vol. 31, no. 1, pp. 64–68, May 2002.

[18] N. Kashtan, S. Itzkovitz, R. Milo, and U. Alon, "Efficient sampling algorithm for estimating subgraph concentrations and detecting network motifs," *Bioinformatics*, vol. 20, no. 11, pp. 1746–1758, Jul. 2004.

[19] S. Patra and A. Mohapatra, "Review of tools and algorithms for network motif discovery in biological networks," *IET Syst. Biol.*, vol. 14, no. 4, pp. 171–189, Aug. 2020.

[20] D. Kim, A. Tran, H. J. Kim, Y. Lin, J. Y. H. Yang, and P. Yang, "Gene regulatory network reconstruction: Harnessing the power of single-cell multi-omic data," *Npj Syst. Biol. Appl.*, vol. 9, no. 1, p. 51, Oct. 2023.

[21] S. Liang, S. Fuhrman, and R. Somogyi, "Reveal, a general reverse engineering algorithm for inference of genetic network architectures," in *Proc. Pac. Symp. Biocomput.*, vol. 3, 1998, pp. 18–29.

[22] X. Zhang et al., "Inferring gene regulatory networks from gene expression data by path consistency algorithm based on conditional mutual information," *Bioinformatics*, vol. 28, no. 1, pp. 98–104, Jan. 2012.

[23] V. Chaitankar, P. Ghosh, E. J. Perkins, P. Gong, Y. Deng, and C. Zhang, "A novel gene network inference algorithm using predictive minimum description length approach," *BMC Syst. Biol.*, vol. 4, no. S1, pp. 1–12, May 2010.

[24] J. S. Fleck et al., "Inferring and perturbing cell fate regulomes in human brain organoids," *Nature*, vol. 621, no. 7978, pp. 365–372, Sep. 2023.

[25] D. Osorio, Y. Zhong, G. Li, J. Z. Huang, and J. J. Cai, "ScTenifoldNet: A machine learning workflow for constructing and comparing transcriptome-wide gene regulatory networks from single-cell data," *Patterns*, vol. 1, no. 9, Dec. 2020, Art. no. 100139.

[26] C. Szegedy et al., "Going deeper with convolutions," in *Proc. 2015 IEEE Conf. Comput. Vis. Pattern Recognit. (CVPR)*, Boston, MA, USA, 2015, pp. 1–9, doi: 10.1109/CVPR.2015.7298594.

[27] Z. Wu, S. Pan, F. Chen, G. Long, C. Zhang, and P. S. Yu, "A comprehensive survey on graph neural networks," *IEEE Trans. Neural Netw. Learn. Syst.*, vol. 32, no. 1, pp. 4–24, Jan. 2021, doi: 10.1109/TNNLS.2020.2978386.

[28] G. Mao et al., "Predicting gene regulatory links from single-cell RNA-seq data using graph neural networks," *Brief. Bioinform.*, vol. 24, no. 6, 2023, Art. no. bbad414.

[29] Y.-H. Wu et al., "Knowledge graph embedding for profiling the interaction between transcription factors and their target genes," *PLOS Comput. Biol.*, vol. 19, no. 6, Jun. 2023, Art. no. e1011207.

[30] J. Zhou, N. Gong, Y. Hu, H. Yu, G. Wang, and H. Wu, "GRANet: A graph residual attention network for gene regulatory network inference," *Briefings Bioinf.*, vol. 26, no. 4, p. 349, Jul. 2025.

[31] H. L. Pahl, "Activators and target genes of Rel/NF-κB transcription factors," *Oncogene*, vol. 18, no. 49, pp. 6853–6866, Nov. 1999.

[32] S. McManus et al., "The transcription factor Pax5 regulates its target genes by recruiting chromatin-modifying proteins in committed B cells," *EMBO J.*, vol. 30, no. 12, pp. 2388–2404, 2011.

[33] K. Harms, S. Nozell, and X. Chen, "The common and distinct target genes of the p53 family transcription factors," *Cellular Mol. Life Sci. (CMLS)*, vol. 61, nos. 7–8, pp. 822–842, Apr. 2004.

[34] S. Wu, K. Jin, M. Tang, Y. Xia, and W. Gao, "Inference of gene regulatory networks based on multi-view hierarchical hypergraphs," *Interdiscipl. Sci., Comput. Life Sci.*, vol. 16, no. 2, pp. 318–332, Jun. 2024.

[35] J. S. Hawe, F. J. Theis, and M. Heinig, "Inferring interaction networks from multi-omics data," *Frontiers Genet.*, vol. 10, p. 535, Jun. 2019.

[36] Y. Zhou, X. Xiao, L. Dong, C. Tang, G. Xiao, and L. Xu, "Cooperative integration of spatially resolved multi-omics data with COSMOS," *Nature Commun.*, vol. 16, no. 1, p. 27, Jan. 2025.

[37] Z. Mei, X. Bi, D. Li, W. Xia, F. Yang, and H. Wu, "DHHNN: A dynamic hypergraph hyperbolic neural network based on variational autoencoder for multimodal data integration and node classification," *Inf. Fusion*, vol. 119, Jul. 2025, Art. no. 103016.

[38] U. Alon, "Network motifs: Theory and experimental approaches," *Nature Rev. Genet.*, vol. 8, no. 6, pp. 450–461, Jun. 2007.

[39] Z. Zhang, Q. Liu, H. Wang, C. Lu, and C.-K. Lee, "Motif-based graph self-supervised learning for molecular property prediction," in *Proc. Adv. Neural Inf. Process. Syst. (NeurIPS)*, vol. 34, 2021, pp. 15870–15882.

[40] J. Liu et al., "MARS: A motif-based autoregressive model for retrosynthesis prediction," *Bioinformatics*, vol. 40, no. 3, p. 115, Mar. 2024.

[41] F. Wang, K. Pena-Pena, W. Qian, and G. R. Arce, "T-HyperGNNs: Hypergraph neural networks via tensor representations," *IEEE Trans. Neural Netw. Learn. Syst.*, vol. 36, no. 3, pp. 5044–5058, Mar. 2025, doi: 10.1109/TNNLS.2024.3371382.

[42] Y. Gao, Y. Feng, S. Ji, and R. Ji, "HGNN+: General hypergraph neural networks," *IEEE Trans. Pattern Anal. Mach. Intell.*, vol. 45, no. 3, pp. 3181–3199, Mar. 2023, doi: 10.1109/TPAMI.2022.3182052.

[43] M. Yang, E. Isufi, M. T. Schaub, and G. Leus, "Simplicial convolutional filters," *IEEE Trans. Signal Process.*, vol. 70, pp. 4633–4649, 2022, doi: 10.1109/TSP.2022.3207045.

[44] T. Gao, W. Liu, and J. Guo, "Simplicial neural networks for biological network analysis," *IEEE Trans. Neural Netw. Learn. Syst.*, vol. 34, no. 2, pp. 647–659, Feb. 2023, doi: 10.1109/TNNLS.2022.3169007.

[45] X. Huang, M. Guo, and J. Han, "Motif convolutional networks," *IEEE Trans. Knowl. Data Eng.*, vol. 33, no. 9, pp. 3658–3670, Aug. 2021, doi: 10.1109/TKDE.2020.3009289.

[46] P. Zhang and J. Tang, "Graph motif convolutional networks for heterogeneous graph learning," *IEEE Trans. Knowl. Data Eng.*, vol. 34, no. 9, pp. 4156–4169, Aug. 2022, doi: 10.1109/TKDE.2021.3059756.

[47] Z. Li, X. Hu, and Y. Zhu, "Efficient hypergraph representation learning for large-scale data," *IEEE Trans. Neural Netw. Learn. Syst.*, 2023, doi: 10.1109/TNNLS.2023.3271234.

[48] D. Zhou, C. Cui, Z. Hu, and S. Yang, "Beyond pairwise graph learning: Hypergraph neural networks and applications," *IEEE Trans. Neural Netw. Learn. Syst.*, early access, 2025, doi: 10.1109/TNNLS.2025.3141592.

[49] A. Pratapa, A. P. Jalihal, J. N. Law, A. Bharadwaj, and T. M. Murali, "Benchmarking algorithms for gene regulatory network inference from single-cell transcriptomic data," *Nature Methods*, vol. 17, no. 2, pp. 147–154, Feb. 2020.

[50] H. Han et al., "TRRUST V2: An expanded reference database of human and mouse transcriptional regulatory interactions," *Nucleic Acids Res.*, vol. 46, no. D1, pp. D380–D386, Jan. 2018.

[51] J. E. Moore et al., "Expanded encyclopaedias of DNA elements in the human and mouse genomes," *Nature*, vol. 583, no. 7818, pp. 699–710, 2020.

[52] D. Szklarczyk et al., "STRING v11: Protein–protein association networks with increased coverage, supporting functional discovery in genome-wide experimental datasets," *Nucleic Acids Res.*, vol. 47, no. D1, pp. D607–D613, Jan. 2019.

[53] H. Zhao, "Ranking users in social networks with higher-order structures," in *Proc. AAAI Conf. Artif. Intell.*, 2018, vol. 32, no. 1, pp. 232–240.

[54] Y. Sun, D. Zhu, H. Du, and Z. Tian, "Motifs-based recommender system via hypergraph convolution and contrastive learning," *Neurocomputing*, vol. 512, pp. 323–338, Nov. 2022.

[55] J. Liu et al., "Graph attention network with convolutional layer for predicting gene regulations from single-cell ribonucleic acid sequence data," *Eng. Appl. Artif. Intell.*, vol. 136, Oct. 2024, Art. no. 108938.

[56] K. Kishan, R. Li, F. Cui, Q. Yu, and A. R. Haake, "GNE: A deep learning framework for gene network inference by aggregating biological information," *BMC Syst. Biol.*, vol. 13, no. S2, pp. 1–14, Apr. 2019.

[57] H. Shu et al., "Modeling gene regulatory networks using neural network architectures," *Nature Comput. Sci.*, vol. 1, no. 7, pp. 491–501, Jul. 2021.

[58] H. Shu et al., "Boosting single-cell gene regulatory network reconstruction via bulk-cell transcriptomic data," *Briefings Bioinf.*, vol. 23, no. 5, p. 389, Sep. 2022.
[59] J. Chen et al., "DeepDRIM: A deep neural network to reconstruct cell-type-specific gene regulatory network using single-cell RNA-seq data," *Briefings Bioinf.*, vol. 22, no. 6, p. 325, Nov. 2021.
[60] Y. Weng, X. Chen, L. Chen, and W. Liu, "GAIN: Graph attention & interaction network for inductive semi-supervised learning over large-scale graphs," *IEEE Trans. Knowl. Data Eng.*, vol. 34, no. 9, pp. 4156–4170, Sep. 2022.

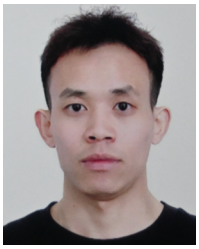

Songyang Wu received the M.S. degree from the School of Information Science and Technology, Yunnan Normal University, Kunming, China, in 2024. He is currently pursuing the Ph.D. degree with the School of Computer and Artificial Intelligence, Southwest Jiaotong University, Chengdu, China.

His research interests include graph representation learning and its applications in bioinformatics, disease diagnosis, and tumor diagnosis.

Mingjing Tang received the Ph.D. degree from the School of Software, Yunnan University, Kunming, China, in 2022.

He is currently a Professor with the School of Information Science and Technology, Yunnan Normal University, Kunming. His main research interests include computational intelligence, graph neural networks, and bioinformatics.

Tong Zi received the B.S. degree from the School of Data Science and Engineering, Kunming City College, Kunming, China, in 2020. He is currently pursuing the master's degree with the School of Information Science and Technology, Yunnan Normal University, Kunming.

His research interests include bioinformatics.

Lin Liu received the Ph.D. degree from the School of Information, Yunnan University, Kunming, China, in 2017.

She is currently a Professor with the School of Information Science and Technology, Yunnan Normal University, Kunming. Her main research interests include computational intelligence and bioinformatics.

Shaojie Qiao received the B.S. and Ph.D. degrees from Sichuan University, Chengdu, China, in 2004 and 2009, respectively.

He is currently a Distinguished Young Scholar of Sichuan Province. He is a Professor with the School of Software Engineering, Chengdu University of Information Technology, Chengdu. He has authored more than 160 high-quality articles, including IEEE TRANSACTIONS ON KNOWLEDGE AND DATA ENGINEERING, IEEE TRANSACTIONS ON NEURAL NETWORKS AND LEARNING SYSTEMS, and IEEE TRANSACTIONS ON CIRCUITS AND SYSTEMS FOR VIDEO TECHNOLOGY. His research interests include databases and artificial intelligence technologies.

Guiguang Ding (Senior Member, IEEE) is currently a tenured Professor with the School of Software, Tsinghua University, Beijing, China. He has authored or co-authored more than 30 articles in top-tier journals, including IEEE TRANSACTIONS ON PATTERN ANALYSIS AND MACHINE INTELLIGENCE, *IEEE Signal Processing Magazine*, and IEEE TRANSACTIONS ON IMAGE PROCESSING. He has presented more than 70 papers at top-tier international conferences, such as CVPR, NeurIPS, and ICML. His research interests include model architecture design and compression, visual semantic recognition and description, transfer learning, and few-shot learning.

Wei Gao received the Ph.D. degree from the Mathematical Department, Soochow University, Suzhou, China, in 2012.

He is currently a Professor at the School of Mathematics, Hohai University, Nanjing, China. He has over more than 300 publications, which report over more than 7000 citations (with an H-index of 45). His research interests include graph theory, networks, statistical learning theory, and artificial intelligence.

Dr. Gao is a Committee Member of China Society of Industrial and Applied Mathematics (CSIAM) Graph Theory and Combinatorics with Applications Committee, and the Chair of ICED in 2017, ISGTCTC 2018, and ISTCS 2019-2025.